Noname manuscript No.
(will be inserted by the editor)

A Stabilized Dual Mixed Hybrid Finite Element Method with Lagrange multipliers for Three-Dimensional Elliptic Problems with Internal Interfaces

Riccardo Sacco · Aurelio Giancarlo Mauri · Giovanna Guidoboni

Received: date / Accepted: date

Abstract This work studies an elliptic boundary value problem with diffusive, advective and reactive terms, in a three-dimensional domain composed of two media separated by a selective interface. For the numerical approximation of the problem we propose a novel approach that combines, for the first time: (1) a dual mixed hybrid (DMH) finite element method (FEM) based on the lowest order Raviart-Thomas space (RT0); (2) a Three-Field (3F) formulation; and (3) a Streamline Upwind/Petrov-Galerkin (SUPG) stabilization method. After proving that the weak formulation of the proposed method and its numerical counterpart are both uniquely solvable and that the finite element scheme enjoys optimal convergence properties with respect to the discretization parameter, we present an efficient implementation based on static condensation, which reduces the method to a nonconforming finite element approach on a grid made by three-dimensional simplices. Extensive computational tests indicate that: (1) the theoretical convergence properties are verified; (2) the DMH-RT0 FEM is accurate and stable even in the presence of marked interface jump discontinuities in the solution and its associated normal flux; and (3) in the case of strongly dominating advective terms, the SUPG stabilization

Riccardo Sacco
Dipartimento di Matematica, Politecnico di Milano,
Piazza Leonardo da Vinci 32, 20133 Milano, Italy
E-mail: riccardo.sacco@polimi.it

Aurelio Giancarlo Mauri
Dipartimento di Matematica, Politecnico di Milano,
Piazza Leonardo da Vinci 32, 20133 Milano, Italy
E-mail: aureliogiancarlo.mauri@polimi.it

Giovanna Guidoboni
Department of Electrical Engineering and Computer Science,
Department of Mathematics,
University of Missouri,
201 Naka Hall, Columbia, MO 65211
E-mail: guidobonig@missouri.edu

resolves accurately steep boundary and/or interior layers without introducing spurious unphysical oscillations or excessive smearing of the solution front.

Keywords Finite element method · mixed hybrid methods · interfaces · transmission problems · stabilization

1 Introduction and motivation

The study of heterogeneous physical systems composed of two or more media separated by selective interfaces is a topic of utmost relevance in applied sciences. Indeed, many applications in biology [32,52,48,13], materials science [42,43,33], nanoelectronics [4] and geophysics [35,2], to name a few, are characterized by interface phenomena that play a crucial role in determining the transmission of physical quantities between different media and/or between different regions within the same medium.

The present work focuses on a class of mathematical problems directly motivated by the aforementioned applications. Specifically, we consider a stationary advection-diffusion-reaction problem in a three-dimensional volume, denoted by $\Omega \subset \mathbb{R}^3$, whose physical properties may vary in space, thereby leading to an elliptic second-order partial differential equation with variable coefficients. In addition, we account for the presence of a selective internal interface, denote by Γ, which is geometrically represented by a two-dimensional manifold in Ω and on which we impose suitable transmission conditions to ensure the balance of flux density across the interface and to model segregation phenomena that may occur within the interface itself. For example, the mathematical setting considered in this article may be used to describe superficial chemical processes involved in semiconductor crystal growth [14] or mass transport and reaction mechanisms occurring at the cellular scale across the membrane lipid bilayer [53].

The fact that many driving processes actually occur at internal interfaces poses serious challenges for the numerical solution of the class of problems described above. In particular, in order to obtain physically-relevant solutions it is crucial to maintain the main physical features associated with interfacial phenomena from the continuous to the discrete level, including the continuity of flux density at the interface. Many numerical approaches have been proposed for the solution of elliptic problems in spatially heterogeneous domains. In particular, domain decomposition methods have been proven to be very effective in dealing with partitions in the volume, which may result from physical heterogeneities in the medium and/or from artificial partitioning aimed at reducing the computational costs of large-scale problems. Many different discretization techniques have been utilized within the context of domain decomposition methods, including finite elements, spectral elements and finite volumes. We refer to [41] for a complete overview of theoretical and computational properties of the domain decomposition approach.

Motivated by the need of accurately capturing interface phenomena, in this work we propose a novel numerical approach that combines, for the first time:

1. a *Dual Mixed Hybrid (DMH) finite element method (FEM)* in order to ensure that: *(i)* the solution and its associated flux satisfy the given partial differential equation within each element (see [45]); *(ii)* the flux is continuous across elements (see [20,44]); and *(iii)* both solution variables satisfy optimal error estimates (see [8,46]);
2. a *Three-Field formulation (3F)*, typical of domain decomposition approaches, in order to account for interfacial discontinuities within the weak formulation of the problem (see [9,41,10]);
3. a *Streamline Upwind/Petrov-Galerkin (SUPG) stabilization method* in order to gain the required amount of numerical stability without significantly spoiling the accuracy of the computed solution due to excessive crosswind smearing (see [11,30]).

The use of hybrid and/or hybridized finite element methods to numerically treat advection-diffusion-reaction problems is not a novel idea of this article. A first example is the high-order hybridizable discontinuous Galerkin (HDG) finite element method proposed in [31] to solve elliptic interface problems in which the solution and gradient are nonsmooth because of jump conditions across the interface. A second example is the robust a posteriori error estimator for the HDG method for convection-diffusion equations with dominant convection proposed in [16]. A third, very recent, example is the a priori error analysis of a HDG method on a family of anisotropic triangulations for a convection-dominated diffusion 2D problem proposed in [12].

While the DMH finite element formulation proposed in this article is certainly connected with the references mentioned above, we remark that it represents an original contribution with respect to other methods as it incorporates in a unified setting the advantages of the mixed-hybrid method, of the 3F method and of the SUPG stabilization. In particular, the pair of Lagrange multipliers introduced within the 3F formulation is a natural fit for the DMH FEM functional framework (see [9,41]), whereas the use of static condensation allows us to eliminate variables defined in the interior of each element in favor of the sole hybrid variable, thereby obtaining a final algebraic system structurally analogous to that of a standard finite element approach (see [6] and [8, Chapter 5]).

The proposed stabilized DMH-RT0 FEM is analyzed at both the infinite and finite dimensional levels, and its well-posedness and optimal error estimates are proved under suitable assumptions on the data. A series of simulations is performed to validate the accuracy and robustness of the novel method via comparison between numerical and analytical solutions in three-dimensional test cases. Results show that the proposed stabilized DMH-RT0 FEM scheme (*i*) satisfies the theoretical findings even in the presence of marked interface jump discontinuities in the solution and its associated flux; and (*ii*) is capable of accurately resolving steep boundary and/or interior layers without introducing spurious unphysical oscillations or excessive smearing of the solution front.

An overview of the article is as follows. Section 2 introduces the mathematical model and the physical meaning of interface and boundary conditions, whereas Section 1 addresses the issue of the well-posedness of the transmission boundary-value problem. Section 4 presents the weak formulation of the problem through the novel DMH method proposed in the article and the analysis of its well-posedness. Section 5 presents the Galerkin approximation of the DMH weak problem studied in Section 4, the analysis of its well-posedness and optimal error estimates for its convergence. Section 6 describes how to introduce a mechanism of stabilization into the DMH-RT0 FEM to prevent the onset of spurious unphysical oscillations when the problem becomes advection-dominated. Section 7 is devoted to the spectral analysis of the stabilized diffusion tensor. Section 8 provides a thorough discussion of the numerical simulations conducted to validate the accuracy and stability of the novel DMH-RT0 FEM. Section 9 gives a summary of the content of the work and an overview of future investigations. Appendix A addresses the issue of how to efficiently implement the proposed DMH-RT0 FEM via static condensation.

2 Mathematical model

Let Ω be an open polyhedral subset of $\mathbb{R}^3$ and let $\partial\Omega \equiv \Sigma$ denote the boundary of Ω on which an outward unit normal vector $\mathbf{n}$ is defined (see Figure 1).

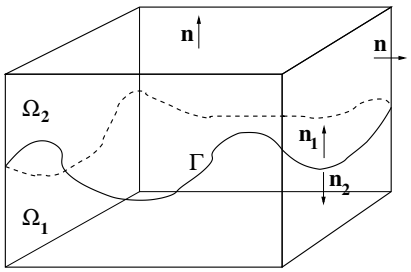

Figure 1 – The domain Ω, its partition into subregions Ω_1, Ω_2, the internal interface Γ and the geometrical notation.

The domain Ω is the union of two subregions Ω_1 and Ω_2, whose boundaries are denoted by $\partial\Omega_1$ and $\partial\Omega_2$, respectively. The two subregions are separated by the interface $\Gamma = \partial\Omega_1 \cap \partial\Omega_2$. For any function $w : \Omega \to \mathbb{R}$, we denote by w_1 and w_2 the restrictions of w to Ω_1 and Ω_2, respectively. We also denote by $w_1|_\Gamma$ and $w_2|_\Gamma$ the traces on Γ of w_1 and w_2, respectively. For each point $\mathbf{y} \in \Gamma$, we define two unit normal vectors $\mathbf{n}_1(\mathbf{y})$ and $\mathbf{n}_2(\mathbf{y})$ outwardly directed with respect to Ω_1 and Ω_2, respectively, for which it holds $\mathbf{n}_1(\mathbf{y}) + \mathbf{n}_2(\mathbf{y}) = \mathbf{0}$.

Thus, the three-dimensional problem considered in this article reads:

$$\begin{aligned}
&\mathrm{div}\mathbf{J} + ru = g && \text{in } (\Omega \setminus \Gamma) && \text{(1a)}\\
&\mathbf{J} = \mathbf{v}u - \boldsymbol{\mu}\nabla u && \text{in } (\Omega \setminus \Gamma) && \text{(1b)}\\
&\mathbf{J}_1|_\Gamma \cdot \mathbf{n}_1 + \mathbf{J}_2|_\Gamma \cdot \mathbf{n}_2 = -\sigma && \text{on } \Gamma && \text{(1c)}\\
&u_2|_\Gamma = \kappa u_1|_\Gamma && \text{on } \Gamma && \text{(1d)}\\
&\gamma\mathbf{J}\cdot\mathbf{n} = \alpha u - \beta && \text{on } \Sigma. && \text{(1e)}
\end{aligned}$$

The dependent variables of the problem are u and the flux density $\mathbf{J}$. Equation (1a) is a stationary conservation law in which the quantity $g-ru$ represents a net production rate of the physical quantity modeled by the function u, with $r = r(\mathbf{x})$ and $g = g(\mathbf{x})$ denoting positive bounded given functions of space. The given advection field $\mathbf{v} = \mathbf{v}(\mathbf{x})$ is assumed to be piecewise smooth over Ω, whereas the diffusivity tensor $\boldsymbol{\mu}$ is assumed to be a multiple of the identity, namely $\boldsymbol{\mu}(\mathbf{x}) = \mu(\mathbf{x})\mathbf{I}$, where $\mathbf{I}$ is the identity tensor in $\mathbb{R}^3$ and the function μ satisfies the following bound

$$0 < \mu_{min} \leq \mu(\mathbf{x}) \leq \mu_{max} < +\infty \qquad \text{for a.e. } \mathbf{x} \in \Omega. \qquad \text{(1f)}$$

Equations (1c) and (1d) are the transmission conditions enforced on the interface Γ. Equation (1c) expresses the balance of flux density across the interface separating the two subdomains, where the given function $\sigma = \sigma(\mathbf{x})$ represents a superficial source ($\sigma > 0$) or sink ($\sigma < 0$) over the interface. Equation (1d) expresses the mechanism of segregation occurring within the interface, where the positive quantity κ represents a local equilibrium constant (see [53] for an application of model (1) (without the advective term) to cellular biology and [15] for an application of model (1) (without the advective term) to semiconductor device technology). Equation (1e) expresses the boundary condition on the external surface of Ω, where α, β and γ are given functions of space such that (1e) corresponds to a Robin boundary condition if $\gamma \neq 0$ and $\alpha \neq 0$, to a Neumann boundary condition if $\gamma \neq 0$ and $\alpha = 0$ and to a Dirichlet boundary condition if $\gamma = 0$ and $\alpha \neq 0$. In the remainder of the article, we assume that $\gamma = 1$ and $\alpha > 0$ on Σ, except in the numerical tests illustrated in Section 8 where $\gamma = 0$ on a subset of Σ.

3 Well-posedness of the transmission problem

The well-posedness of the transmission boundary-value problem (1) depends strongly on the values of κ and σ. In the case where $\kappa = 1$ and $\sigma = 0$, the well-posedness analysis can be conducted using standard techniques based on the weak formulation of (1), and the subsequent adoption of the Lax-Milgram Lemma, to determine the conditions on model coefficients under which the transmission problem admits a unique solution u depending continously on the data (see [34], [27] and [40, Chapter 5]). In the case where $\kappa \neq 1$ and $\sigma \neq 0$, the well-posedness analysis becomes a nontrivial issue because the transmission

conditions (1c) and (1d) do not allow to deal *only* with the dependent variable u *but* necessarily require the introduction of other dependent variables defined on the interface Γ. An example of weak formulation of problem (1) that ideally fits the case $\kappa \neq 1$ and $\sigma \neq 0$ is represented by the Three-Field approach (3F), which was originally proposed and studied in [9] in the context of domain-decomposition methods and subsequently analyzed in [41] and [10].

Since a theoretical analysis of well-posedness of the weak formulation of a boundary-value problem in the form of (1) is, to the best of our knowledge, still lacking, and the focus of this work is to introduce, analyze and validate a novel numerical scheme, we leave to a future research the proof of well-posedness of (1) and make the following assumption.

Assumption 1 (Well-posedness of the transmission problem (1)**)** *We assume that there exists a unique function u satisfying the equations, transmission and boundary conditions in* (1) *and depending continously on the data.*

4 Dual mixed hybrid weak formulation

The weak formulation of problem (1) is obtained by extending the DMH method (see [50,44,22,23,25]) to include Lagrange multipliers for the interface conditions (1c) and (1d), in the spirit of the 3F formulation (see [9,41, 10]). For the sake of clarity, we begin by describing the functional setting in Section 4.1, followed by the geometrical discretization of the domain in Section 4.2, the derivation of the weak formulation in Section 4.3 and the study of its well-posedeness in Section 4.4.

4.1 Functional setting

Let us denote by $\mathcal{S}$ an open bounded subset of $\mathbb{R}^3$ having a boundary $\partial\mathcal{S}$. Throughout the article, we will utilize the functional spaces $L^2(\mathcal{S})$, $H^1(\mathcal{S})$ and $H(\mathrm{div};\mathcal{S})$, endowed with the usual L^2-, H^1- and $H(\mathrm{div})-$ norms denoted by $\|\cdot\|_{0,\mathcal{S}}$, $\|\cdot\|_{1,\mathcal{S}}$ and $\|\cdot\|_{H(\mathrm{div};\mathcal{S})}$, respectively, with div denoting the divergence operator. We refer to [50,46,8] and references cited therein for definitions and mathematical properties of the above mentioned functional spaces. In addition, we will denote by $(\cdot,\cdot)_{\mathcal{S}}$ the scalar product in L^2 over $\mathcal{S}$ and, for simplicity, we will use the shortened notation $(\cdot,\cdot)_i$ for the scalar product in L^2 over Ω_i.

4.2 Geometrical discretization

Let $\{\mathcal{T}_h\}_{h>0}$ denote a family of regular triangulations of the computational domain Ω made of closed tetrahedral elements K (cf. Definition 3.4.1 of [40]), where the positive quantity h represents the discretization parameter. We assume that each partition of the family satisfies the admissibility criteria of [40],

Section 3.1. We also assume that each subdomain Ω_i, $i = 1, 2$, is exactly covered by the elements of $\mathcal{T}_h$ and we denote by $\mathcal{T}_{h,1}$ and $\mathcal{T}_{h,2}$ the restrictions of $\mathcal{T}_h$ to Ω_1 and Ω_2, in such a way that $\Omega = \mathcal{T}_{h,1} \cup \mathcal{T}_{h,2}$ and $\Gamma = \mathcal{T}_{h,1} \cap \mathcal{T}_{h,2}$. This latter property amounts to assuming that the two partitions connect in a *conforming* manner at the interface. For more general geometrical approaches and related numerical schemes, we refer to [41] in the context of domain decomposition methods, to [18] in the context of Hybridizable Discontinuous Galerkin finite elements and to [26] in the context of Extended finite element methods.

For every $K \in \mathcal{T}_h$, we denote by h_K the diameter of K and we let $h := \max_{K \in \mathcal{T}_h} h_K$. We denote by ∂K the boundary of K and by $\mathbf{n}_{\partial K}$ the outward unit normal vector on ∂K. An interior face of $\mathcal{T}_h$ is a planar set F of 2-dimensional positive measure defined as $F := \partial K_1 \cap \partial K_2$ for some two elements K_1 and K_2 belonging to $\mathcal{T}_h$. We say that F is a boundary face of $\mathcal{T}_h$ if there exists an element $K \in \mathcal{T}_h$ such that $F = \partial K \cap \Sigma$ and the 2-dimensional measure of F is positive. We introduce the following sets of faces:

- $\mathcal{F}_{h,int}$: the set of faces belonging to the interior of Ω but not to Γ;
- $\mathcal{F}_{h,\Gamma}$: the set of faces belonging to Γ;
- $\mathcal{F}_{h,\Sigma}$: the set of faces belonging to the domain boundary Σ;
- $\mathcal{F}_h$: the union of all the faces in $\mathcal{F}_{h,int}$, $\mathcal{F}_{h,\Gamma}$ and $\mathcal{F}_{h,\Sigma}$.

The set $\mathcal{F}_{h,int}$ can be divided into the sum of the two disjoint sets $\mathcal{F}_{h,int,1}$ (faces in the interior of Ω_1) and $\mathcal{F}_{h,int,2}$ (faces in the interior of Ω_2). Analogously, $\mathcal{F}_{h,\Sigma}$ can be divided into the sum of the two disjoint sets $\mathcal{F}_{h,\Sigma_1}$ (faces on Σ_1) and $\mathcal{F}_{h,\Sigma_2}$ (faces on Σ_2). According to these definitions we have:

$$\mathcal{F}_{h,int} = \mathcal{F}_{h,int,1} \cup \mathcal{F}_{h,int,2}, \tag{2a}$$

$$\mathcal{F}_{h,\Sigma} = \mathcal{F}_{h,\Sigma_1} \cup \mathcal{F}_{h,\Sigma_2}, \tag{2b}$$

$$\mathcal{F}_h = \mathcal{F}_{h,int} \cup \mathcal{F}_{h,\Gamma} \cup \mathcal{F}_{h,\Sigma}. \tag{2c}$$

We also define the sets:

$$\mathcal{F}_{h,1} = \mathcal{F}_{h,int,1} \cup \mathcal{F}_{h,\Sigma_1} \cup \mathcal{F}_{h,\Gamma}, \tag{3a}$$

$$\mathcal{F}_{h,2} = \mathcal{F}_{h,int,2} \cup \mathcal{F}_{h,\Sigma_2} \cup \mathcal{F}_{h,\Gamma}. \tag{3b}$$

4.3 The DMH weak formulation

For every set $\mathcal{S} \in \mathbb{R}^3$, let us introduce the following subspace of $H(\mathrm{div}; \mathcal{S})$

$$\mathcal{H}(\mathrm{div}; \mathcal{S}) := \left\{ \mathbf{q} \in H(\mathrm{div}; \mathcal{S}) \,|\, \mathbf{q} \cdot \mathbf{n}_{\partial \mathcal{S}} \in L^2(\partial \mathcal{S}) \right\} \subset H(\mathrm{div}; \mathcal{S}). \tag{4}$$

Then, for $i = 1, 2$, we introduce the following spaces:

$$\mathbf{V}_i = \left\{ \mathbf{v} \in (L^2(\Omega_i))^3,\, \mathbf{v}_K \in \mathcal{H}(\mathrm{div}; K)\, \forall K \in \mathcal{T}_{h,i} \right\}, \tag{5a}$$

$$V_i = L^2(\Omega_i), \tag{5b}$$

$$M_i = L^2(\mathcal{F}_{h,i}), \tag{5c}$$

$$M_{J,i} = L^2(\mathcal{F}_{h,\Gamma}), \tag{5d}$$

$$M_\lambda = L^2(\mathcal{F}_{h,\Gamma}). \tag{5e}$$

Remark 1 Functions in M_1 and M_2 are single-valued on each face belonging to the interior of $\mathcal{T}_{h,1}$ and $\mathcal{T}_{h,2}$ and on each face belonging to Σ_1 and Σ_2. On the contrary, on each face F belonging to $\mathcal{F}_{h,\Gamma}$ we have, in general, $\mu_1|_F \neq \mu_2|_F$, $\mu_1 \in M_1$, $\mu_2 \in M_2$. This property allows us to represent a jump discontinuity of the trace of a function across the interface Γ and is the reason why the faces on Γ are attributed to both sets $\mathcal{F}_{h,1}$ and $\mathcal{F}_{h,2}$ in the definitions (3a)- (3b). The same argument holds for functions belonging to the spaces $M_{J,1}$ and $M_{J,2}$.

We set $\mathcal{V} := \mathbf{V}_1 \times V_1 \times \mathbf{V}_2 \times V_2$, $\mathcal{Q} := M_1 \times M_2 \times M_{J,1} \times M_{J,2} \times M_\lambda$, and we define $\mathtt{u} := (\mathbf{J}_1, u_1, \mathbf{J}_2, u_2) \in \mathcal{V}$, $\mathtt{p} := (\widehat{u}_1, \widehat{u}_2, \mathcal{J}_1, \mathcal{J}_2, \lambda) \in \mathcal{Q}$, $\mathtt{v} := (\boldsymbol{\tau}_1, \phi_1, \boldsymbol{\tau}_2, \phi_2) \in \mathcal{V}$ and $\mathtt{q} := (\mu_1, \mu_2, \rho_1, \rho_2, \varphi) \in \mathcal{Q}$. We endow $\mathcal{V}$ and $\mathcal{Q}$ with the following norms:

$$\|\mathtt{u}\|_{\mathcal{V}} = \Big(\sum_{K\in\mathcal{T}_{h,1}} \|\mathbf{J}_1\|^2_{H(\mathrm{div};K)} + \sum_{K\in\mathcal{T}_{h,2}} \|\mathbf{J}_2\|^2_{H(\mathrm{div};K)} + \|u_1\|^2_{0,\Omega_1} + \|u_2\|^2_{0,\Omega_2} \Big)^{1/2}, \tag{6a}$$

$$\|\mathtt{p}\|_{\mathcal{Q}} = \Big(\sum_{F\in\mathcal{F}_{h,1}} \|\widehat{u}_1\|^2_{0,F} + \sum_{F\in\mathcal{F}_{h,2}} \|\widehat{u}_2\|^2_{0,F} + \sum_{F\in\mathcal{F}_{h,\Gamma}} \|\mathcal{J}_1\|^2_{0,F} + \sum_{F\in\mathcal{F}_{h,\Gamma}} \|\mathcal{J}_2\|^2_{0,F} + \sum_{F\in\mathcal{F}_{h,\Gamma}} \|\lambda\|^2_{0,F} \Big)^{1/2}. \tag{6b}$$

For all $\mathtt{u} \in \mathcal{V}$, $\mathtt{v} \in \mathcal{V}$, and for all $\mathtt{p} \in \mathcal{Q}$, $\mathtt{q} \in \mathcal{Q}$, we introduce the following bilinear forms and linear functionals:

$$\begin{aligned} a(\mathtt{u},\mathtt{v}) :=& (\boldsymbol{\mu}^{-1}\mathbf{J}_1, \boldsymbol{\tau}_1)_1 - (\boldsymbol{\mu}^{-1}\mathbf{v}u_1, \boldsymbol{\tau}_1)_1 + (ru_1, \phi_1)_1 \\ &- \sum_{K\in\mathcal{T}_{h,1}} (u_1, \mathrm{div}\boldsymbol{\tau}_1)_K + \sum_{K\in\mathcal{T}_{h,1}} (\phi_1, \mathrm{div}\mathbf{J}_1)_K \\ &+ (\boldsymbol{\mu}^{-1}\mathbf{J}_2, \boldsymbol{\tau}_2)_2 - (\boldsymbol{\mu}^{-1}\mathbf{v}u_2, \boldsymbol{\tau}_2)_2 + (ru_2, \phi_2)_2 \\ &- \sum_{K\in\mathcal{T}_{h,2}} (u_2, \mathrm{div}\boldsymbol{\tau}_2)_K + \sum_{K\in\mathcal{T}_{h,2}} (\phi_2, \mathrm{div}\mathbf{J}_2)_2, \end{aligned} \tag{7a}$$

$$b(\mathtt{u},\mathtt{q}) := \sum_{K\in\mathcal{T}_{h,1}} (\mathbf{J}_1\cdot\mathbf{n}_{\partial K}, \mu_1)_{\partial K} + \sum_{K\in\mathcal{T}_{h,2}} (\mathbf{J}_2\cdot\mathbf{n}_{\partial K}, \mu_2)_{\partial K}, \tag{7b}$$

$$\begin{aligned} c(\mathtt{p},\mathtt{q}) :=& \sum_{F\in\mathcal{F}_{h,\Sigma_1}} (\alpha\widehat{u}_1, \mu_1)_F + \sum_{F\in\mathcal{F}_{h,\Sigma_2}} (\alpha\widehat{u}_2, \mu_2)_F \\ &- \sum_{F\in\mathcal{F}_{h,\Gamma}} (\rho_1, \widehat{u}_1)_F - \sum_{F\in\mathcal{F}_{h,\Gamma}} (\rho_2, \widehat{u}_2)_F \\ &+ \sum_{F\in\mathcal{F}_{h,\Gamma}} (\rho_1, \lambda)_F + \sum_{F\in\mathcal{F}_{h,\Gamma}} (\rho_2, \kappa\lambda)_F \\ &+ \sum_{F\in\mathcal{F}_{h,\Gamma}} (\mathcal{J}_1, \mu_1)_F + \sum_{F\in\mathcal{F}_{h,\Gamma}} (\mathcal{J}_2, \mu_2)_F \\ &- \sum_{F\in\mathcal{F}_{h,\Gamma}} (\mathcal{J}_1, \varphi)_F - \sum_{F\in\mathcal{F}_{h,\Gamma}} (\mathcal{J}_2, \varphi)_F, \end{aligned} \tag{7c}$$

$$L(\mathtt{v}) := (g, \phi_1)_1 + (g, \phi_2)_2, \tag{7d}$$

$$G(\mathtt{q}) := -\sum_{F\in\mathcal{F}_{h,\Sigma_1}} (\beta, \mu_1)_F - \sum_{F\in\mathcal{F}_{h,\Sigma_2}} (\beta, \mu_2)_F - \sum_{F\in\mathcal{F}_{h,\Gamma}} (\sigma, \varphi)_F. \tag{7e}$$

The DMH weak formulation of problem (1) then reads:

Given the linear functionals $L : \mathcal{V} \to \mathbb{R}$ and $G : \mathcal{Q} \to \mathbb{R}$, find $\mathtt{u} = (\mathbf{J}_1, u_1, \mathbf{J}_2, u_2) \in \mathcal{V}$ and $\mathtt{p} = (\widehat{u}_1, \widehat{u}_2, \mathcal{J}_1, \mathcal{J}_2, \lambda) \in \mathcal{Q}$ such that:

$$a(\mathtt{u},\mathtt{v}) + b(\mathtt{v},\mathtt{p}) = L(\mathtt{v}) \qquad \forall \mathtt{v} = (\boldsymbol{\tau}_1, \phi_1, \boldsymbol{\tau}_2, \phi_2) \in \mathcal{V}, \tag{8a}$$

$$b(\mathtt{u},\mathtt{q}) - c(\mathtt{p},\mathtt{q}) = G(\mathtt{q}) \qquad \forall \mathtt{q} = (\mu_1, \mu_2, \rho_1, \rho_2, \varphi) \in \mathcal{Q}, \tag{8b}$$

where $\mathcal{V} := \mathbf{V}_1 \times V_1 \times \mathbf{V}_2 \times V_2$, $\mathcal{Q} := M_1 \times M_2 \times M_{J,1} \times M_{J,1} \times M_\lambda$ and the bilinear forms a, b and c are defined in (7).

Remark 2 System (8) is in the form of a generalized saddle-point problem as considered in [8, Sect. II.1.2] and [46, Remark 10.8]. We notice that $a(\cdot,\cdot)$ and $b(\cdot,\cdot)$ are the standard bilinear forms in a dual mixed hybrid formulation of a second-order boundary value problem with an advection-diffusion-reaction operator (see [21,5]). On the contrary, the bilinear form $c(\cdot,\cdot)$ and the right-hand side $G(\cdot)$ contain the contributions of the Lagrange multipliers, borrowed from

the 3F formulation, which allow us to enforce the transmission conditions (1c) and (1d). These contributions represent a novel aspect of the DMH method proposed in this article.

4.4 Unique solvability of the DMH weak formulation

The following theorem is the main result of this section.

Theorem 1 (Uniqueness of the solution of (8)) *Let* $\mathbf{v} \in (L^\infty(\Omega))^3$, $r \in L^\infty(\Omega)$, $g \in L^2(\Omega)$, *and* $\alpha \in L^\infty(\Sigma)$. *Assume that:*

$$0 < r_{min} \le r(\mathbf{x}) \le r_{max} < +\infty \qquad \text{for a.e. } \mathbf{x} \in \Omega, \tag{9a}$$

$$0 < \alpha_{min} \le \alpha(\mathbf{x}) \le \alpha_{max} < +\infty \qquad \text{for a.e. } \mathbf{x} \in \Sigma. \tag{9b}$$

$$\frac{\|\mathbf{v}\|_{\infty,\Omega}}{2\mu_{min}} < \min\left\{\mu_{max}^{-1}, r_{min}\right\}. \tag{9c}$$

Then, the DMH weak formulation (8) *of problem* (1) *is uniquely solvable.*

Proof The proof proceeds as in the proof of Proposition 1.7.1 of [41]. It is straightforward to see that if the pair u_i, $i = 1, 2$, is the solution of (1) (which exists and is unique in virtue of Assumption 1, then the pair $(\mathtt{u}, \mathtt{p}) = ((\mathbf{J}_1, u_1, \mathbf{J}_2, u_2), (\widehat{u}_1, \widehat{u}_2, \mathcal{J}_1, \mathcal{J}_2, \lambda))$ is a solution of (8). Uniqueness follows by inspecting the homogeneous problem, i.e., we set $g = \sigma = \beta = 0$ in (8). Let us consider Equation (8b) and take $\mathtt{q} = [\mu_1|_\Gamma, 0, 0, 0, 0]^T$. This yields $\mathcal{J}_1 = \mathbf{J}_1 \cdot \mathbf{n}_1$ on Γ. Similarly, taking $\mathtt{q} = [0, \mu_2|_\Gamma, 0, 0, 0]^T$ we get $\mathcal{J}_2 = \mathbf{J}_2 \cdot \mathbf{n}_2$ on Γ. Finally, taking $\mathtt{q} = [0, 0, 0, 0, \varphi]^T$ yields $\mathcal{J}_1 + \mathcal{J}_2 = 0$ on Γ which in turn gives

$$\mathbf{J}_1 \cdot \mathbf{n}_1 + \mathbf{J}_2 \cdot \mathbf{n}_2 = 0 \qquad \text{on } \Gamma. \tag{10a}$$

Taking $\mathtt{q} = [0, 0, \rho_1, 0, 0]^T$ yields $\lambda = \widehat{u}_1$ on Γ whereas taking $\mathtt{q} = [0, 0, 0, \rho_2, 0,]^T$ yields $\widehat{u}_2 = \kappa\lambda$ from which we conclude that

$$\widehat{u}_2 = \kappa\widehat{u}_1 \qquad \text{on } \Gamma. \tag{10b}$$

Taking $\mathtt{q} = \left[\mu_1|_{\mathcal{F}_{h,int,1} \cup \mathcal{F}_{h,\Sigma_1}}, 0, 0, 0, 0\right]^T$ yields:

$$\mathbf{J}_1 \in H(\mathrm{div}; \Omega_1), \tag{10c}$$

$$\mathbf{J}_1 \cdot \mathbf{n} = \alpha\widehat{u}_1 \qquad \text{on } \Sigma_1. \tag{10d}$$

whereas taking $\mathtt{q} = \left[0, \mu_2|_{\mathcal{F}_{h,int,2} \cup \mathcal{F}_{h,\Sigma_2}}, 0, 0, 0\right]^T$ yields:

$$\mathbf{J}_2 \in H(\mathrm{div}; \Omega_2), \tag{10e}$$

$$\mathbf{J}_2 \cdot \mathbf{n} = \alpha\widehat{u}_2 \qquad \text{on } \Sigma_2. \tag{10f}$$

Let us now consider Equation (8a) and take $\mathtt{v} = [\mathbf{J}_1, u_1, 0, 0]^T$. This yields

$$(\mu^{-1}\mathbf{J}_1, \mathbf{J}_1)_1^2 - (\mu^{-1}\mathbf{v}u_1, \mathbf{J}_1)_1 + (ru_1, u_1)_1^2 + \sum_{K \in \mathcal{T}_{h,1}} (\widehat{u}_1, \mathbf{J}_1 \cdot \mathbf{n}_{\partial K})_{\partial K} = 0.$$

Using (10c) and (10d) in the last term of the previous relation yields

$$(\mu^{-1}\mathbf{J}_1,\mathbf{J}_1)_1^2-(\mu^{-1}\mathbf{v}u_1,\mathbf{J}_1)_1+(ru_1,u_1)_1^2+(\widehat{u}_1,\mathbf{J}_1\cdot\mathbf{n}_1)_\Gamma+(\alpha\widehat{u}_1,\widehat{u}_1)_{\Sigma_1}=0. \tag{10g}$$

Taking $\mathtt{v}=[0,0,\mathbf{J}_2,u_2]^T$ and proceeding similarly as above, we get

$$(\mu^{-1}\mathbf{J}_2,\mathbf{J}_2)_2^2-(\mu^{-1}\mathbf{v}u_2,\mathbf{J}_2)_2+(ru_2,u_2)_2^2+\sum_{K\in\mathcal{T}_{h,2}}(\widehat{u}_2,\mathbf{J}_2\cdot\mathbf{n}_{\partial K})_{\partial K}=0.$$

Using (10e), (10f) and (10b) in the last term of the previous relation yields

$$(\mu^{-1}\mathbf{J}_2,\mathbf{J}_2)_2^2-(\mu^{-1}\mathbf{v}u_2,\mathbf{J}_2)_2+(ru_2,u_2)_1^2-\kappa(\widehat{u}_1,\mathbf{J}_1\cdot\mathbf{n}_1)_\Gamma+(\alpha\widehat{u}_2,\widehat{u}_2)_{\Sigma_2}=0. \tag{10h}$$

Let us elaborate Equation (10g). Using (1f), (9a), (9b) and Cauchy-Schwarz inequality we obtain

$$\begin{aligned}&(\mu^{-1}\mathbf{J}_1,\mathbf{J}_1)_1^2-(\mu^{-1}\mathbf{v}u_1,\mathbf{J}_1)_1+(ru_1,u_1)_1^2+(\alpha\widehat{u}_1,\widehat{u}_1)_{\Sigma_1}\\&\geq\mu_{max}^{-1}\|\mathbf{J}_1\|_{L^2(\Omega_1)}^2-\mu_{min}^{-1}\|\mathbf{v}\|_{L^\infty(\Omega)}\|u_1\|_{L^2(\Omega_1)}\|\mathbf{J}_1\|_{L^2(\Omega_1)}\\&+r_{min}\|u_1\|_{L^2(\Omega_1)}^2+\alpha_{min}\|\widehat{u}_1\|_{L^2(\Sigma_1)}^2.\end{aligned}$$

Using Young's inequality in the second term of the previous relation and assumption (9c), we finally get

$$\begin{aligned}H_1&:=(\mu^{-1}\mathbf{J}_1,\mathbf{J}_1)_1^2-(\mu^{-1}\mathbf{v}u_1,\mathbf{J}_1)_1+(ru_1,u_1)_1^2+(\alpha\widehat{u}_1,\widehat{u}_1)_{\Sigma_1}\\&\geq C\left(\|\mathbf{J}_1\|_{L^2(\Omega_1)}^2+\|u_1\|_{L^2(\Omega_1)}^2+\|\widehat{u}_1\|_{L^2(\Sigma_1)}^2\right)\geq 0,\end{aligned} \tag{10i}$$

where

$$C=\min\left\{\mu_{max}^{-1}-\frac{\|\mathbf{v}\|_{L^\infty(\Omega)}}{2\mu_{min}},\,r_{min}-\frac{\|\mathbf{v}\|_{L^\infty(\Omega)}}{2\mu_{min}},\alpha_{min}\right\}.$$

Proceeding similarly with Equation (10h), we get

$$\begin{aligned}H_2&:=(\mu^{-1}\mathbf{J}_2,\mathbf{J}_2)_2^2-(\mu^{-1}\mathbf{v}u_2,\mathbf{J}_2)_2+(ru_2,u_2)_2^2+(\alpha\widehat{u}_2,\widehat{u}_2)_{\Sigma_2}\\&\geq C\left(\|\mathbf{J}_2\|_{L^2(\Omega_2)}^2+\|u_2\|_{L^2(\Omega_2)}^2+\|\widehat{u}_2\|_{L^2(\Sigma_2)}^2\right)\geq 0.\end{aligned} \tag{10j}$$

Using inequality (10i) into (10g) yields

$$(\widehat{u}_1,\mathbf{J}_1\cdot\mathbf{n}_1)_\Gamma=-H_1\leq 0,$$

whereas using inequality (10j) into (10h) yields

$$(\widehat{u}_1,\mathbf{J}_1\cdot\mathbf{n}_1)_\Gamma=\frac{1}{\kappa}H_2\geq 0,$$

which obviously yields $H_1=H_2=0$, implying

$$\mathbf{J}_1=\mathbf{J}_2=\mathbf{0},\qquad u_1=u_2=0,\qquad \widehat{u}|_\Sigma=0.$$

Taking now $\mathtt{v} = \left[\boldsymbol{\tau}^*_{1,K}, 0, 0, 0\right]^T$ in Equation (8a), with $\boldsymbol{\tau}^*_{1,K} \cdot \mathbf{n}_{\partial K} = \widehat{u}_1|_{\partial K}$ for all $K \in \mathcal{T}_{h,1}$, yields

$$(\widehat{u}_1, \widehat{u}_1)_{\partial K} = 0 \qquad \forall K \in \mathcal{T}_{h,1}$$

which implies $\widehat{u}_1 = 0$ on $\mathcal{F}_{h,int,1} \cup \Gamma$. Proceeding similarly with Equation (8b), we obtain $\widehat{u}_2 = 0$ on $\mathcal{F}_{h,int,2} \cup \Gamma$. This concludes the proof. □.

Let $\xi = \xi(\mathtt{q})$ be a given linear functional defined on $\mathcal{Q}$ and define the affine manifold

$$\mathcal{V}^\xi := \{\mathtt{v} \in \mathcal{V},\ b(\mathtt{v}, \mathtt{q}) = \xi(\mathtt{q})\ \forall \mathtt{q} \in \mathcal{Q}\}\,. \tag{11a}$$

Setting $\xi = 0$ we obtain the characterization the kernel of the abstract operator associated with the form b

$$\mathcal{V}^0 := \{\mathtt{v} \in \mathcal{V},\ b(\mathtt{v}, \mathtt{q}) = 0\ \forall \mathtt{q} \in \mathcal{Q}\}\,. \tag{11b}$$

Remark 3 Having proved that (8) is uniquely solvable, given $\mathtt{p} \in \mathcal{Q}$, we set

$$\mathcal{H}(\mathtt{q}) := G(\mathtt{q}) + c(\mathtt{p}, \mathtt{q}) \qquad \forall \mathtt{q} \in \mathcal{Q}, \tag{12}$$

and we see that (8) can be written in the equivalent form:
Given $L \in \mathcal{V}'$, find $\mathtt{u} \in \mathcal{V}^{\mathcal{H}}$ such that

$$a(\mathtt{u}, \mathtt{v}) = L(\mathtt{v}) \qquad \forall \mathtt{v} \in \mathcal{V}^0. \tag{13}$$

This formula is the counterpart of Eq. (7.4.8) of [40].

5 The DMH Galerkin finite element approximation

In this section we illustrate the Galerkin finite element approximation of the weak DMH formulation of problem (1). To this end, in Section 5.1 we introduce the local and global finite element spaces. Then, in Section 5.2 we prove that the DMH formulation admits a unique solution and exhibits optimal convergence with respect to the discretization parameter h.

5.1 Finite element spaces

For any set $\mathcal{S}$ (in one, two or three spatial dimensions), we indicate by $\mathbb{P}_r(\mathcal{S})$, $r \geq 0$, the space of polynomials of degree $\leq r$ defined on $\mathcal{S}$. Moreover, we define $RT_0(K) := (\mathbb{P}_0(K))^3 \oplus \mathbb{P}_0(K)\mathbf{x}$ and we define the following local polynomial spaces associated with the triangulation $\mathcal{T}_h$:

$$\mathbf{V}(K) := \{\mathbf{v} \in RT_0(K)\ \forall K \in \mathcal{T}_h\}\,, \tag{14a}$$

$$V(K) := \{v \in \mathbb{P}_0(K)\ \forall K \in \mathcal{T}_h\}\,, \tag{14b}$$

$$M(F) := \{\mu \in \mathbb{P}_0(F)\ \forall F \in \mathcal{F}_h\}\,. \tag{14c}$$

In order to construct the finite dimensional spaces associated with (14) to be used for the internal approximation of the functional spaces (5), we distinguish between the spaces of functions defined inside each element of $\mathcal{T}_h$ and the spaces of functions defined on each face of $\mathcal{F}_h$. For $i = 1, 2$, we have:

$$\mathbf{V}_{i,h} = \{\boldsymbol{\tau} \in \mathbf{V}_i,\, \boldsymbol{\tau}|_K \in \mathbf{V}(K)\ \forall K \in \mathcal{T}_{h,i}\}\,,\ i = 1, 2, \tag{15a}$$
$$V_{i,h} = \{\phi \in V_i,\, \phi|_K \in V(K)\ \forall K \in \mathcal{T}_{h,i}\}\,,\ i = 1, 2, \tag{15b}$$
$$M_{i,h} = \{\mu \in M_i,\, \mu|_F \in M(F)\ \forall F \in \mathcal{F}_{h,i}\}\,,\ i = 1, 2, \tag{15c}$$
$$M_{J,i,h} = \{\mu \in M_{J,i},\, \mu|_F \in M(F)\ \forall F \in \mathcal{F}_{h,\Gamma,i}\}\,,\ i = 1, 2, \tag{15d}$$
$$M_{\lambda,h} = \{\mu \in M_\Lambda,\, \mu|_F \in M(F)\ \forall F \in \mathcal{F}_{h,\Gamma}\}\,. \tag{15e}$$

Having defined the global finite element spaces on the partitioned triangulation, we can define the global spaces on $\mathcal{T}_h$ as:

$$\mathcal{V}_h := \mathbf{V}_{1,h} \times V_{1,h} \times \mathbf{V}_{2,h} \times V_{2,h}, \tag{16a}$$
$$\mathcal{Q}_h := M_{1,h} \times M_{2,h} \times M_{J,1,h} \times M_{J,2,h} \times M_{\lambda,h}. \tag{16b}$$

5.2 The DMH numerical method

The DMH-RT0 FE approximation of problem (1) reads:
Given $L_h = L(\mathtt{v}_h)$ and $G_h = G(\mathtt{q}_h)$, find $\mathtt{u}_h = (\mathbf{J}_{1,h}, u_{1,h}, \mathbf{J}_{2,h}, u_{2,h}) \in \mathcal{V}_h$ and $\mathtt{p}_h = (\widehat{u}_{1,h}, \widehat{u}_{2,h}, \mathcal{J}_{1,h}, \mathcal{J}_{2,h}, \lambda_h) \in \mathcal{Q}_h$ such that:

$$a(\mathtt{u}_h, \mathtt{v}_h) + b(\mathtt{v}_h, \mathtt{p}_h) = L_h \qquad \forall \mathtt{v}_h = (\boldsymbol{\tau}_{1,h}, \phi_{1,h}, \boldsymbol{\tau}_{2,h}, \phi_{2,h}) \in \mathcal{V}_h, \tag{17a}$$
$$b(\mathtt{u}_h, \mathtt{q}_h) - c(\mathtt{p}_h, \mathtt{q}_h) = G_h \qquad \forall \mathtt{q}_h = (\mu_{1,h}, \mu_{2,h}, \rho_{1,h}, \rho_{2,h}, \varphi_h) \in \mathcal{Q}_h, \tag{17b}$$

where the bilinear forms $a(\cdot,\cdot)$, $b(\cdot,\cdot)$ and $c(\cdot,\cdot)$, and the linear functionals $L(\cdot)$, $G(\cdot)$ are defined in (7), whereas the spaces $\mathcal{V}_h$ and $\mathcal{Q}_h$ are defined in (16).

5.3 Unique solvability, error estimates and convergence of the DMH-RT0 FE approximation

In this section we first prove that the DMH-RT0 FE approximation of problem (1) admits a unique solution. Then, we establish error estimates for the approximate formulation using the Babuska-Brezzi theory for the analysis of saddle-point problems (see [40, Chapter 7]). Finally, we use the approximation theory for hybrid methods developed in [46] and [6] to prove the optimal convergence of the DMH-RT0 FE method with respect to the discretization parameter h.

Theorem 2 (Unique solvability of (17)**)** *Under the same assumptions as in Theorem 1, the DMH-RT0 FE approximation* (17) *of problem* (1) *has a unique solution.*

Proof The proof of the uniqueness of the solution of (17) is the copy of that of Theorem 1 provided to replace $\mathtt{u}$, $\mathtt{v}$, $\mathtt{p}$ and $\mathtt{q}$ with the corresponding discrete versions, with the only following differences:

$$\mathbf{J}_{1,h} \cdot \mathbf{n}|_F = P_{0,F}\alpha\, \widehat{u}_{1,h} \qquad \forall F \in \Sigma_1. \tag{18}$$

instead of (10d), and

$$\mathbf{J}_{2,h} \cdot \mathbf{n}|_F = P_{0,F}\alpha\, \widehat{u}_{2,h} \qquad \forall F \in \Sigma_2. \tag{19}$$

instead of (10f), having denoted by $P_{0,F}$ the L^2-projection over the space $\mathbb{P}_0(F)$, F being a face of $\mathcal{T}_h$. □.

As in the infinite dimensional case, let $\xi_h = \xi(\mathtt{q}_h)$ be a given linear functional defined on $\mathcal{Q}_h$ and define the affine manifold

$$\mathcal{V}_h^{\xi} := \{\mathtt{v}_h \in \mathcal{V}_h,\ b(\mathtt{v}_h, \mathtt{q}_h) = \xi(\mathtt{q}_h)\ \forall \mathtt{q}_h \in \mathcal{Q}_h\}\,. \tag{20a}$$

Setting $\xi_h = 0$ we obtain the characterization the kernel of the operator associated with the discretization of the form b

$$\mathcal{V}_h^{0} := \{\mathtt{v}_h \in \mathcal{V}_h,\ b(\mathtt{v}_h, \mathtt{q}_h) = 0\ \forall \mathtt{q}_h \in \mathcal{Q}_h\}\,. \tag{20b}$$

Remark 4 In analogy with Remark 3, having proved that (17) is uniquely solvable, given $\mathtt{p}_h \in \mathcal{Q}_h$, we set

$$\mathcal{H}_h(\mathtt{q}_h) := G(\mathtt{q}_h) + c(\mathtt{p}_h, \mathtt{q}_h) \qquad \forall \mathtt{q}_h \in \mathcal{Q}_h, \tag{21}$$

and we see that (17) can be written in the equivalent form:
Given $L \in \mathcal{V}'$, find $\mathtt{u}_h \in \mathcal{V}^{\mathcal{H}_h}$ such that

$$a(\mathtt{u}_h, \mathtt{v}_h) = L(\mathtt{v}_h) \qquad \forall \mathtt{v}_h \in \mathcal{V}_h^0. \tag{22}$$

This formula is the counterpart of Eq. (7.4.21) of [40].

The next theorem provides a priori bounds for the discretization error in terms of the approximation error. Essential ingredients to prove this result are Theorems 1 and 2 which allow us to reformulate the generalized saddle-point problems (8) and (17) into the standard setting (13) and (22), as stated in Remarks 3 and 4. This, in turn, allows us to apply the classical Babuska-Brezzi theory for saddle-point problems (see [40, Chapter 7]) and conclude our theoretical analysis of the DMH approximation of problem (1).

Theorem 3 (Error estimates) *There exist positive constants C_i, $1 = 1, \ldots, 4$, independent of h such that the following optimal error estimates hold:*

$$\|\mathtt{u} - \mathtt{u}_h\|_{\mathcal{V}} \le C_1 \inf_{\mathtt{v}_h \in \mathcal{V}_h} \|\mathtt{u} - \mathtt{v}_h\|_{\mathcal{V}} + C_2 \inf_{\mathtt{q}_h \in \mathcal{Q}_h} \|\mathtt{p} - \mathtt{q}_h\|_{\mathcal{Q}} \tag{23a}$$

$$\|\mathtt{p} - \mathtt{p}_h\|_{\mathcal{Q}} \le C_3 \inf_{\mathtt{v}_h \in \mathcal{V}_h} \|\mathtt{u} - \mathtt{v}_h\|_{\mathcal{V}} + C_4 \inf_{\mathtt{q}_h \in \mathcal{Q}_h} \|\mathtt{p} - \mathtt{q}_h\|_{\mathcal{Q}}. \tag{23b}$$

Proof To prove the error estimates (23) we apply Theorem 7.4.3 of [40]. The proof essentially consists in two steps that are repeated for the continuous formulation (8) and the approximate formulation (17). The first step requires to prove that the bilinear form a is coercive on $\mathcal{V}^0$ (resp., $\mathcal{V}_h^0$) whereas the second step requires to prove the inf-sup condition for the bilinear form b on $\mathcal{V} \times \mathcal{Q}$ (resp., $\mathcal{V}_h \times \mathcal{Q}_h$).

Coercivity of a over $\mathcal{V}^0$. We need to show that there exists a positive constant C_a such that

$$a(\mathtt{U},\mathtt{U}) \geq C_a \|\mathtt{U}\|^2_{\mathcal{V}} \qquad \forall \mathtt{U} \in \mathcal{V}^0, \tag{24}$$

where $\mathcal{V}^0$, the kernel space of $\mathcal{V}$, is given by

$$\begin{aligned}\mathcal{V}^0 = \{&(\mathbf{q}_1,\mathbf{q}_2) \in (\mathcal{H}(\mathrm{div};\Omega_1)\times\mathcal{H}(\mathrm{div};\Omega_2)),\\ &\text{with } \mathrm{div}\mathbf{q}_i = 0, \text{ and } \mathbf{q}_i\cdot\mathbf{n}|_{\partial\Omega_i} = 0,\ i=1,2\}\,.\end{aligned} \tag{25}$$

Using the proof of Theorem 1 it is easy to see that under the assumptions (9c), inequality (24) is satisfied by taking

$$C_a = \min\left\{\mu^{-1}_{max} - \frac{\|\mathbf{v}\|_{L^\infty(\Omega)}}{2\mu_{min}},\, r_{min} - \frac{\|\mathbf{v}\|_{L^\infty(\Omega)}}{2\mu_{min}}\right\}.$$

Inf-sup condition for b over $\mathcal{V}\times\mathcal{Q}$. We need to show that the bilinear form b satisfies the following inf-sup condition

$$\begin{aligned}&\exists k_b > 0 \,\text{such that } \forall \mathtt{q} = [\mu_1,\mu_2,0,0,0,]^T \in \mathcal{Q},\ \exists \mathtt{v_q} \in \mathcal{V} \,\text{such that}\\ &b(\mathtt{v_q},\mathtt{q}) \geq k_b \|\mathtt{v_q}\|_{\mathcal{V}} \|\mathtt{q}\|_{L^2(\Sigma)}.\end{aligned} \tag{26}$$

To prove (26) we consider for each $K \in \mathcal{T}_h$ the auxiliary boundary value problem

$$-\triangle w_i + w_i = 0 \qquad \text{in } K \in \mathcal{T}_{h,i} \quad i=1,2, \tag{27a}$$

$$w_i = \mu_i \qquad \text{on } \partial K \quad i=1,2, \tag{27b}$$

where the function $\mu : \mathcal{F}_h \to \mathbb{R}$ is the trace of the function $w : \Omega \to \mathbb{R}$ whose restriction $w_i = w|_{\Omega_i}$ belongs to the broken space

$$H^1_{\mathcal{T}_{h,i}}(\Omega_i) = \prod_{K\in\mathcal{T}_{h,i}} H^1(K) \qquad i=1,2.$$

Let us set $\mathbf{J}_i = \nabla w_i$ and $\mathtt{v_q}|_K = [\mathbf{J}_i,\, 0]^T$ for all $K \in \mathcal{T}_{h,i}$, $i=1,2$, Using (27a) we see that $\mathrm{div}\mathbf{J}_i = w_i$ for all $K \in \mathcal{T}_{h,i}$, $i=1,2$. Then, a straightforward application of the Lax-Milgram Lemma to (27) and of the trace inequality over Ω_1 and Ω_2 yields

$$\begin{aligned}b(\mathtt{v_q},\mathtt{q}) &= \|w_1\|^2_{H^1_{\mathcal{T}_{h,1}}(\Omega_1)} + \|w_2\|^2_{H^1_{\mathcal{T}_{h,2}}(\Omega_2)}\\ &\geq \|\mathtt{v_q}\|_{\mathcal{V}} \left(C_1^*\|\mu_1\|^2_{L^2(\partial\Omega_1)} + C_2^*\|\mu_2\|^2_{L^2(\partial\Omega_2)}\right)^{1/2}\\ &\geq (C^*)^{1/2}\|\mathtt{v_q}\|_{\mathcal{V}}\|\mathtt{q}\|_{L^2(\Sigma)},\end{aligned} \tag{28}$$

where C_1^* and C_2^* are the trace constants associated with the domains Ω_1 and Ω_2 whereas $C^* = \min\{C_1^*,\, C_2^*\}$. From (28) we see that (26) is satisfied taking $k_b = (C^*)^{1/2}$.

Coercivity of a over $\mathcal{V}_h^0$. We need to show that there exists a positive constant $C_{a,h}$ such that

$$a(\mathtt{U}_h, \mathtt{U}_h) \geq C_{a,h} \|\mathtt{U}_h\|_{\mathcal{V}}^2 \qquad \forall \mathtt{U}_h \in \mathcal{V}_h^0, \tag{29}$$

where $\mathcal{V}_h^0$, the kernel space of $\mathcal{V}_h$, is given by

$$\begin{aligned}\mathcal{V}_h^0 = \{&(\mathbf{q}_1, \mathbf{q}_2) \in (\mathbf{V}_{1,h} \times \mathbf{V}_{2,h}) \cap (\mathcal{H}(\mathrm{div}; \Omega_1) \times \mathcal{H}(\mathrm{div}; \Omega_2)), \\ &\text{with } \mathrm{div}\mathbf{q}_i = 0, \text{ and } \mathbf{q}_i \cdot \mathbf{n}|_{\partial\Omega_i} = 0,\ i = 1, 2\}\,.\end{aligned}$$

Since $\mathcal{V}_h^0 \subset \mathcal{V}^0$ we see that (29) is satisfied by taking $C_{a,h} = C_a$.

Inf-sup condition for b over $\mathcal{V}_h \times \mathcal{Q}_h$. We need to show that the bilinear form b satisfies the following discrete inf-sup condition

$$\begin{aligned}&\exists k_{b,h} > 0 \,\text{such that } \forall \mathtt{q}_h = [\mu_{1,h}, \mu_{2,h}, 0, 0, 0,]^T \in \mathcal{Q}_h,\ \exists \mathtt{v}_{\mathtt{q},h} \in \mathcal{V}_h \,\text{such that} \\ &b(\mathtt{v}_{\mathtt{q},h}, \mathtt{q}_h) \geq k_{b,h} \|\mathtt{v}_{\mathtt{q},h}\|_{\mathcal{V}} \|\mathtt{q}_h\|_{L^2(\Sigma)}.\end{aligned} \tag{30}$$

The discrete inf-sup condition can be proved by using the following abstract result (see [40, Lemma 7.4.1]).

Lemma 1 (Fortin's Lemma) *Assume that there exists an operator $T_h : \mathcal{V} \to \mathcal{V}_h$ and a positive constant k^* independent of h such that:*

$$b(\mathtt{v} - T_h(\mathtt{v}), \mathtt{q}) = 0 \qquad \forall \mathtt{v} \in \mathcal{V},\ \mathtt{q} = [\mu_1, \mu_2, 0, 0, 0,]^T \in \mathcal{Q}. \tag{31a}$$

$$\|T_h(\mathtt{v})\|_{\mathcal{V}} \leq k^* \|\mathtt{v}\|_{\mathcal{V}} \qquad \forall \mathtt{v} \in \mathcal{V}. \tag{31b}$$

Then, the discrete inf-sup condition (30) *is satisfied by taking $k_{b,h} = k_b/k^*$.*

Choosing T_h as the interpolation operator onto the space $\mathbf{V}_{1,h} \times \mathbf{V}_{2,h}$ allows us to verify (31a) by exploting the definition of degrees of freedom of a function in $\mathbf{V}_{1,h} \times \mathbf{V}_{2,h}$ and to prove (31b) proceeding as in the proof of Lemma 7.2.1 of [40]. Since all the assumptions of Theorem 7.4.3 of [40] are satisfied, we obtain the error estimates (23). □.

Using in (23) the approximation theory for hybrid methods developed in [46] yields the following convergence estimates for the DMH-RT0 FEM.

Theorem 4 (Convergence of the DMH-RT0 FEM) *There exist positive constants $C_{\mathtt{u}}$ and $C_{\mathtt{p}}$, independent of h, such that:*

$$\|\mathtt{u} - \mathtt{u}_h\|_{\mathcal{V}} \leq C_{\mathtt{u}}\, h, \tag{32a}$$

$$\|\mathtt{p} - \mathtt{p}_h\|_{\mathcal{Q}} \leq C_{\mathtt{p}}\, h. \tag{32b}$$

Moreover, using the techniques of [6] and [46, Section 21], we can prove the following post-processing error estimates.

Theorem 5 (Convergence of post-processed quantities) *There exist positive constants $\widetilde{C}_1$ and $\widetilde{C}_2$, independent of h, such that:*

$$\|P_0 u - u_h\|_{0,\Omega} \leq \widetilde{C}_1\, h^2, \tag{33a}$$

$$\|u - u_h^*\|_{0,\Omega} \leq \widetilde{C}_2\, h^2, \tag{33b}$$

where $P_0 u$ is the L^2 projection of u on $V_{i,h}$ and u_h^* is the piecewise linear nonconforming interpolant of $\widehat{u}_h$ over $\mathcal{T}_h$ [19].

Remark 5 The error estimates (33) are superconvergence results for the DMH-RT0 FEM. In particular, error estimate (33a) tells us that u_h is a very good approximation of u at the barycenter of each element $K \in \mathcal{T}_h$, whereas error estimate (33b) tells us that the piecewise linear nonconforming interpolant of $\widehat{u}_h$ over the mesh approximates the exact solution u with the same accuracy as that of the piecewise linear solution computed by the standard finite element method applied to problem (1).

6 Artificial diffusion stabilization

In this section we describe one of the novel contributions of this article to the theory and development of dual mixed hybrid methods, namely, the introduction of a stabilization mechanism that ensures numerical robustness to the scheme in the case of advection-dominated regimes, a situation that is particularly relevant in the application of problem (1) to realistic problems of mass transport in heterogeneous domains. To quantitatively characterize the weight of advection with respect to the diffusion, for each element $K \in \mathcal{T}_h$, we set $\overline{\mathbf{v}}_K := \mathbf{v}(\mathbf{x}_{B,K})$, where $\mathbf{x}_{B,K}$ is the barycenter of K, and we define the *local Pèclet number* as

$$\mathrm{Pe}_K := \max_{i=1,\ldots,6} \frac{|\overline{\mathbf{v}}_K \cdot \mathbf{e}_i|}{2\mu}, \tag{34}$$

where $\mathbf{e}_i$, $i = 1, \ldots, 6$, is the vector connecting two vertices of K. Relation (34) extends to the case of tetrahedral elements the definition given in [1] in the case of triangular elements. If $\mathrm{Pe}_K < 1$ the problem is locally diffusion-dominated whereas if $\mathrm{Pe}_K > 1$ the problem is locally advection-dominated. In this latter case, an effective approach to prevent the onset of numerical instabilities consists of introducing an *artificial diffusion tensor* $\boldsymbol{\mu}_K^*$ constructed in such a way to locally increase the diffusion mechanism. Following [7,39] and [40, Chapter 6], the modified diffusion tensor to be used in the artificial diffusion method is defined as

$$(\boldsymbol{\mu}_h)_K = \boldsymbol{\mu}_K + \boldsymbol{\mu}_K^* = \mu \mathbf{I} + \boldsymbol{\mu}_K^*. \tag{35}$$

The effect of numerical dissipation is minimized if artificial diffusion is added *only* in the streamline direction, as done in the Streamline Upwind Petrov-Galerkin method introduced in [11]. To follow this approach, if $|\overline{\mathbf{v}}_K| \neq 0$, we

define the *streamline unit vector*

$$\boldsymbol{\beta}_K := \frac{\overline{\mathbf{v}}_K}{|\overline{\mathbf{v}}_K|} \tag{36a}$$

and set

$$\boldsymbol{\mu}_K^* := \mu \Phi(\mathrm{Pe}_K) \boldsymbol{\beta}_K \boldsymbol{\beta}_K^T. \tag{36b}$$

The amount of artificial diffusion depends on the *stabilization function* Φ that is required to satisfy the following properties:

$$\Phi(X) > 0 \qquad \forall X > 0, \tag{36c}$$

$$\lim_{X \to 0^+} \Phi(X) = 0^+. \tag{36d}$$

We refer to [47] for the illustration and analysis of several choices for Φ. In the numerical examples reported in Section 8 we use the following form of the stabilization function

$$\Phi(X) := X - 1 + \mathtt{Be}(2X), \tag{36e}$$

where $\mathtt{Be}(t) := t/(e^t - 1)$ is the inverse of the Bernoulli function. The choice (36e) satisfies properties (36c)- (36d), and in particular it can be seen that

$$\lim_{h_K \to 0} \Phi(\mathrm{Pe}_K) = \mathcal{O}(h_K^2). \tag{36f}$$

The above relation shows that the artificial diffusion based on (36e) decreases quadratically as the mesh size becomes small, and because of this asymptotic behavior the choice (36e) is referred to as *optimal* artificial diffusion (see [11] and [39]). Another popular choice of Φ, that is also implemented in the numerical examples reported in Section 8, is the so-called Upwind method for which

$$\Phi(X) := X. \tag{36g}$$

The upwind stabilization based on (36g) introduces an artificial diffusion that decreases only linearly as the mesh size becomes small, therefore worsening the accuracy of the computed solution. On the other hand, when Pe_K becomes large, the optimal artificial diffusion and upwind stabilizations practically coincide, thereby supporting the use of (36e) in all regimes instead of (36g) (see also [7] for further discussion of this issue).

7 Spectral analysis of the stabilized diffusion tensor

In this section we study the spectrum of the stabilized diffusion tensor (35) as a function of the transport parameters that characterize the problem at hand. The analysis is carried out for the stabilization function (36e) but similar considerations apply to the stabilization function (36g). Denoting by Λ_i and $\mathbf{X}_i$, $i = 1, 2, 3$, the eigenvalues and the corresponding eigenvectors of $(\boldsymbol{\mu}_h)_K$, an explicit computation yields

$$\Lambda_1 = \Lambda_2 = \mu,\ \Lambda_3 = \mu(1 + \Phi(\mathrm{Pe}_K)), \tag{37a}$$

$$\mathbf{X}_1 = \left[-\frac{\beta_{K,y}}{\beta_{K,x}},\, 1,\, 0\right]^T, \tag{37b}$$

$$\mathbf{X}_2 = \left[-\frac{\beta_{K,z}}{\beta_{K,x}},\, 0,\, 1\right]^T, \tag{37c}$$

$$\mathbf{X}_3 = \left[\frac{\beta_{K,x}}{\beta_{K,z}},\, \frac{\beta_{K,y}}{\beta_{K,z}},\, 1\right]^T. \tag{37d}$$

The stabilized diffusion tensor is a symmetric positive definite 3×3 matrix. Replacing (36e) into the expression of Λ_3 we obtain

$$\Lambda_3 = \mu(\mathrm{Pe}_K + \mathtt{Be}(2\mathrm{Pe}_K)). \tag{37e}$$

If the local Pèclet number is very small, a Taylor expansion of $\mathtt{Be}(2\mathrm{Pe}_K)$ in the neighbourhood of 0 yields $\Lambda_3 = \mu$, so that $(\boldsymbol{\mu}_h)_K$ coincides with $\boldsymbol{\mu}_K = \mu\mathbf{I}$, as expected, because the problem is *not* advection-dominated and thus no stabilization is actually needed. Conversely, if the local Pèclet number is much larger than 1 the quantity $\mathtt{Be}(2\mathrm{Pe}_K)$ can be neglected in (37e), yielding

$$\Lambda_3 \simeq \mu\mathrm{Pe}_K \gg \{\Lambda_1,\, \Lambda_2\}\,. \tag{37f}$$

Therefore, in the case where problem (1) is locally advection-dominated the three-dimensional surface representing the spectrum of the stabilized diffusion tensor in the euclidean space $\mathbb{R}^3$ is an ellipsoid centered in the origin, with the x_1 and x_2 principal axes of equal length and with a strongly elongated principal axis x_3.

Example 1 Consider the reference tetrahedron with vertices $[0,0,0]^T$, $[1,0,0]^T$, $[0,1,0]^T$ and $[0,0,1]^T$. Assume that $\mathbf{v}_K = [0,\, 0,\, 1]^T$ and that $\mu = 10^{-2}$. Using (34) we get $\mathrm{Pe}_K = 50$, which means that the model is in the advection-dominated regime. The artificial diffusion tensor is

$$\boldsymbol{\mu}_K^* = \begin{bmatrix} 0 & 0 & 0 \\ 0 & 0 & 0 \\ 0 & 0 & \mu\Phi(2\mathrm{Pe}_K) \simeq 0.49 \end{bmatrix},$$

which shows that the stabilization introduces a contribution *only* along the z axis that is the streamline direction.

8 Numerical results

In this section we perform a thorough validation of the performance of the proposed method. To this end, we have implemented problem (1) and the DMH-RT0 FEM within the computational software MP-FEMOS (Multi-Physics Finite Element Modeling Oriented Simulator) that has been developed by one of the authors [37,36,3,38,49]. MP-FEMOS is a general-purpose modular code based on the Galerkin Finite Element Method that is programmed in a fully 3D framework through shared libraries using an object-oriented language (C++). Several situations are addressed. In Section 8.1 the accuracy of the scheme is studied in two different cases, corresponding to non active and active interface. In Section 8.2 the stability of the scheme is studied in different regimes, corresponding to low and high local Pèclet numbers. In all test cases, the simulation domain is the unit cube $(0,1) \times (0,1) \times (0,1)$ with the interface at $z = 0.5$. Dirichlet boundary conditions are applied at the bottom and top faces of the cube, with $u = 0$ at the bottom and $u = 1$ at the top, whereas homogeneous Neumann conditions are imposed for $\mathbf{J}$ on the lateral surface.

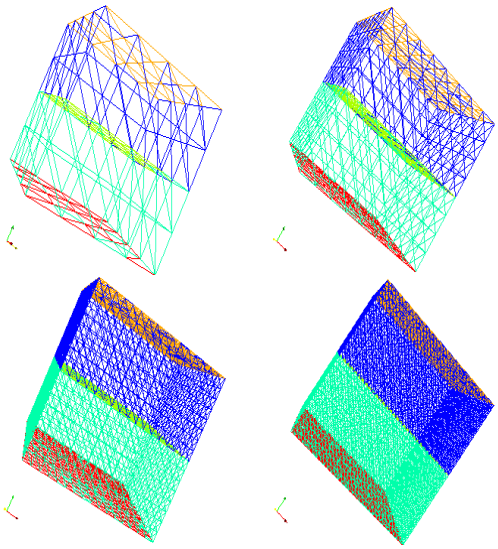

Figure 2 – Regular triangulations with $h = [0.4330, 0.2165, 0.1083, 0.0541]$.

In the computational examples illustrated in Section 8.1, the four tetrahedral meshes shown in Figure 2 are used. Partitions are made of regular elements, with $h = [0.4330, 0.2165, 0.1083, 0.0541]$. For any piecewise smooth function $\eta_h : \mathcal{T}_h \to \mathbb{R}$, we set

$$\|\eta_h\|_{\infty,h} := \max_{K \in \mathcal{T}_h} |\eta_h(\mathbf{x}_{B,K})|.$$

8.1 Convergence analysis

In Section 8.1.1 we study the accuracy of the DMH-RT0 FEM in the case where both u and $\mathbf{J}\cdot\mathbf{n}$ are continuous at Γ. In Section 8.1.2 we consider the case where both u and $\mathbf{J}\cdot\mathbf{n}$ are discontinuous at Γ. All test cases considered in Section 8.1 are conducted in a regime where the Pèclet number is less than 1 and so the scheme is implemented without stabilization. The effect of stabilization will be assessed in Section 8.2.

8.1.1 Non active interface

Let us set $\mu = 1$, $r = 1$, $g = 1$, $\mathbf{v} = v_z\mathbf{e}_3$, $v_z = 1$, $\kappa = 1$ and $\sigma = 0$, where $\mathbf{e}_3$ denotes the unit vector of the z-axis shown in Figure 3. The exact solution of system (1) is the pair:

$$u(z) = \frac{g}{r} + C_1 e^{\lambda_1 z} + C_2 e^{\lambda_2 z} \qquad z \in [0,1] \quad (38a)$$

$$J(z) = \frac{v_z g}{r} + C_1 e^{\lambda_1 z}\,(v_z - \mu\lambda_1) + C_2 e^{\lambda_2 z}\,(v_z - \mu\lambda_2) \qquad z \in [0,1] \quad (38b)$$

$$\mathbf{J}(z) = J(z)\mathbf{e}_3 \qquad z \in [0,1], \quad (38c)$$

where $\lambda_{1,2} = (v_z \pm \sqrt{v_z^2 + 4r\mu})/(2\mu)$ and

$$C_1 = \frac{-1 + \frac{g}{r}(1 - e^{\lambda_2})}{e^{\lambda_2} - e^{\lambda_1}}, \qquad C_2 = \frac{1 - \frac{g}{r}(1 - e^{\lambda_1})}{e^{\lambda_2} - e^{\lambda_1}}.$$

Figure 3 (left panel) illustrates the errors associated with the scalar variable u whereas Figure 3 (right panel) shows the errors associated with the vector variable $\mathbf{J}$. Results indicate that: (i) the DMH formulation is linearly converging with respect to (w.r.t.) the graph norm in the $L^2 \times H(\mathrm{div})$-topology; (ii) u_h quadratically converges to the value of u at the barycenters of $\mathcal{T}_h$; and (iii) $\widehat{u}_h$ quadratically converges to the value of u w.r.t. the discrete maximum norm and the L^2 norm. These outcomes are in complete agreement with the theoretical estimates of Section 5.2 and with existing theoretical estimates for the DMH formulation applied to the solution of elliptic boundary value problems on a single domain (see [6,21,8,5]).

8.1.2 Active interface

Let us set $\mu = 1$, $r = 1$, $g = 1$, $\mathbf{v} = v_z\mathbf{e}_3$, $v_z = 1$, as in the previous section, and let us set $\kappa = 2$ and $\sigma = 1$ to model the active interface. The exact solution of

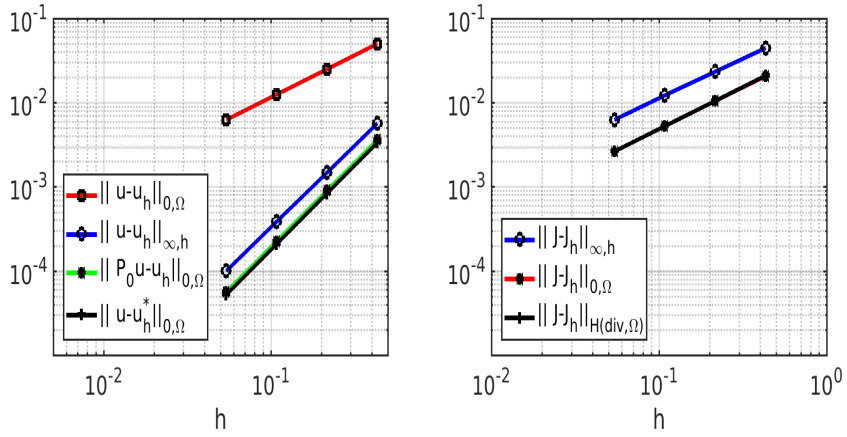

Figure 3 – Error curves for the DMH-RT0 FEM. The values of model coefficients are: $\mu = 1$, $r = 1$, $g = 1$, $\mathbf{v} = v_z\mathbf{e}_3$, $v_z = 1$, $\kappa = 1$ and $\sigma = 0$. Left panel: $\|u - u_h\|_{0,\Omega}$ (red curve); $\|u - u_h\|_{\infty,h}$ (blue curve); $\|P_0u - u_h\|_{0,\Omega}$ (green curve); $\|u - u_h^*\|_{0,\Omega}$ (black curve). Right panel: $\|\mathbf{J} - \mathbf{J}_h\|_{\infty,h}$ (blue curve); $\|\mathbf{J} - \mathbf{J}_h\|_{0,\Omega}$ (red curve); $\|\mathbf{J} - \mathbf{J}_h\|_{H(\mathrm{div};\Omega)}$ (black curve).

system (1) is the pair:

$$u(z) = \frac{g}{r} + C_1 e^{\lambda_1 z} + C_2 e^{\lambda_2 z} \qquad z \in [0, 0.5) \qquad (39a)$$

$$J(z) = \frac{v_z g}{r} + C_1 e^{\lambda_1 z}\,(v_z - \mu\lambda_1) + C_2 e^{\lambda_2 z}\,(v_z - \mu\lambda_2) \qquad z \in [0, 0.5), \qquad (39b)$$

$$u(z) = \frac{g}{r} + C_3 e^{\lambda_1 z} + C_4 e^{\lambda_2 z} \qquad z \in [0.5, 1] \qquad (39c)$$

$$J(z) = \frac{v_z g}{r} + C_3 e^{\lambda_1 z}\,(v_z - \mu\lambda_1) + C_4 e^{\lambda_2 z}\,(v_z - \mu\lambda_2) \qquad z \in [0.5, 1], \qquad (39d)$$

where $\lambda_{1,2} = (v_z \pm \sqrt{v_z^2 + 4r\mu})/(2\mu)$ and the four constants C_k, $k = 1, 2, 3, 4$ are the solutions of the following linear system

$$\mathcal{C}\mathbf{c} = \mathbf{g},$$

where $\mathbf{c} = [C_1, C_2, C_3, C_4]^T$,

$$\mathcal{C} = \begin{bmatrix} 1 & 1 & 0 & 0 \\ e^{\lambda_1/2}(v_z - \mu\lambda_1) & e^{\lambda_2/2}(v_z - \mu\lambda_2) & -e^{\lambda_1/2}(v_z - \mu\lambda_1) & -e^{\lambda_2/2}(v_z - \mu\lambda_2) \\ -\kappa e^{\lambda_1/2} & -\kappa e^{\lambda_2/2} & e^{\lambda_1/2} & e^{\lambda_2/2} \\ 0 & 0 & e^{\lambda_1} & e^{\lambda_2} \end{bmatrix},$$

and

$$\mathbf{g} = \begin{bmatrix} -\dfrac{g}{r} \\ -\sigma \\ (\kappa - 1)\dfrac{g}{r} \\ 1 - \dfrac{g}{r} \end{bmatrix}.$$

The error curves obtained for this problem are shown in Figure 4. Results are very similar to those obtained in the case of a nonactive interface.

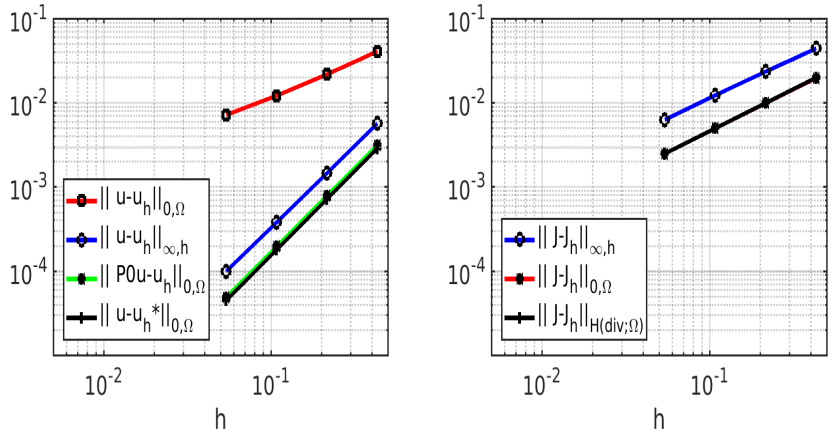

Figure 4 – Error curves for the DMH-RT0 FEM. The values of model coefficients are: $\mu = 1$, $r = 1$, $g = 1$, $\mathbf{v} = v_z\mathbf{e}_3$, $v_z = 1$, $\kappa = 2$ and $\sigma = 1$. Left panel: $\|u - u_h\|_{0,\Omega}$ (red curve); $\|u - u_h\|_{\infty,h}$ (blue curve); $\|P_0u - u_h\|_{0,\Omega}$ (green curve); $\|u - u_h^*\|_{0,\Omega}$ (black curve). Right panel: $\|\mathbf{J} - \mathbf{J}_h\|_{\infty,h}$ (blue curve); $\|\mathbf{J} - \mathbf{J}_h\|_{0,\Omega}$ (red curve); $\|\mathbf{J} - \mathbf{J}_h\|_{H(\mathrm{div};\Omega)}$ (black curve).

A three-dimensional view of the solutions u_h and $J_{h,z}$ computed by the DMH-RT0 FEM is reported in Figure 5 whereas Figure 6 shows a a cross-sectional view of the along the z-axis of the same computed quantities. Results indicate that the method is able to accurately capture the jump discontinuity even with a rather coarse partition of the domain.

8.2 The effect of stabilization

In this section we carry out a verification of the effect of the streamline artificial diffusion on the stability properties of the DMH method in the presence of a dominating advective term. The tetrahedral mesh is the same in all the tested cases with $h = 0.108253$.

8.2.1 Non active interface

Here we treat the case where the interface is not active and so we consider the same parameters as in Section 8.1.1 where, in particular, $\kappa = 1$ and $\sigma = 0$. Figure 7 shows a cross-sectional view of the reconstructed solution u_h^* along the z-axis in correspondance of six increasing values of the local Pèclet number obtained with the following data: value nr. 1: $\mu = 0.5$, $v_z = 1$; value nr. 2: $\mu = 0.0125$, $v_z = 0.625$; values from nr. 3 to nr. 6: $v_z = 0.625$ and $\mu = \{6.25 \cdot 10^{-3}, 3.125 \cdot 10^{-3}, 1.5625 \cdot 10^{-3}, 7.8125 \cdot 10^{-4}\}$.

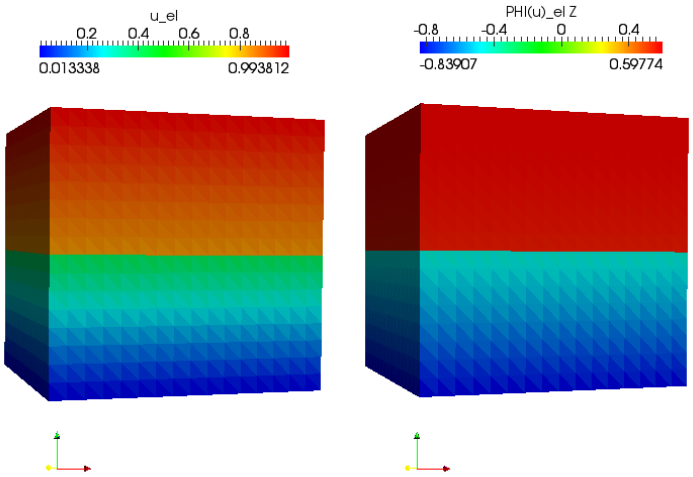

Figure 5 – 3D color plots of the solutions computed by the DMH-RT0 FEM. Left panel: values of u_h at the barycenter of each element. Right panel: values of $J_{z,h}$ at the barycenter of each element.

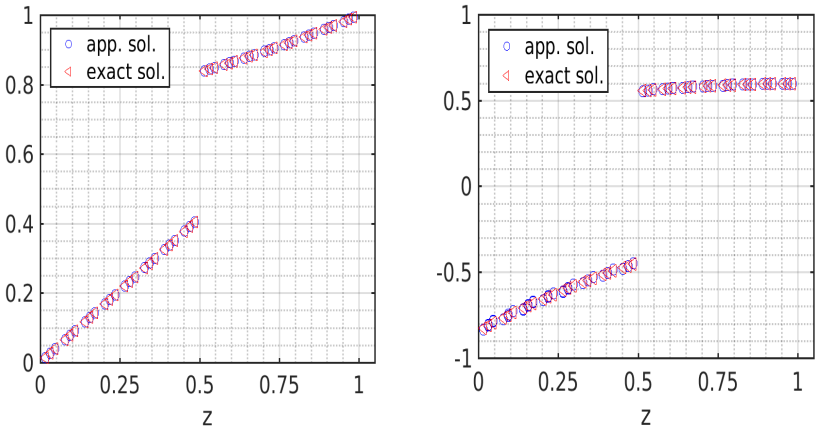

Figure 6 – 1D plots of the solutions computed by the DMH-RT0 FEM along the z-axis. Left panel: values of u_h at the barycenter of each element. Right panel: values of $J_{z,h}$ at the barycenter of each element.

Results show that as Pe_K increases, the non stabilized method starts to display spurious unphysical oscillations in the boundary layer region, which tend to propagate backwards throughout the computational domain because of the markedly hyperbolic behavior of the problem. On the contrary, the stabilized method is characterized by a robust behavior with respect to the increase of the local Pèclet number, showing in particular that the SG stabilized DMH

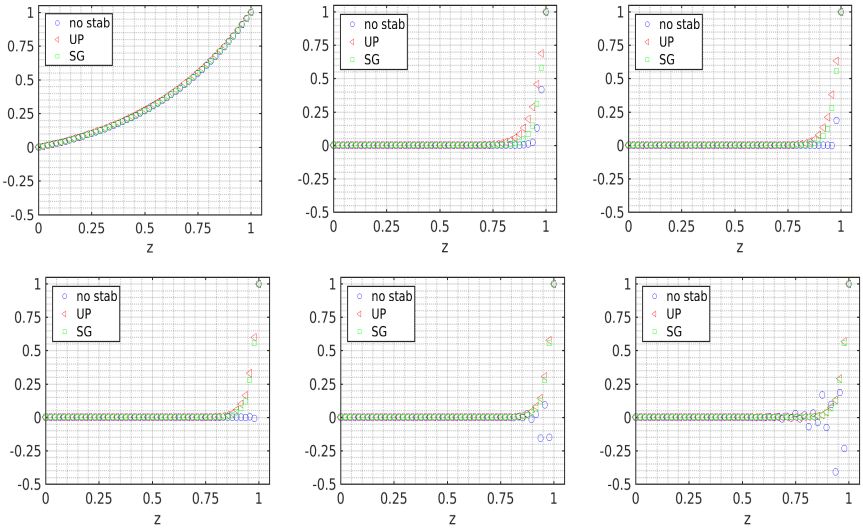

Figure 7 – 1D plot of the computed solution u_h^* along the z-axis. Blue circles: unstabilized solution. Green squares: SG stabilization. Red triangles: Upwind stabilization. Top row. left panel: $\mathrm{Pe}_K = 0.1083$; middle panel: $\mathrm{Pe}_K = 2.7063$; right panel: $\mathrm{Pe}_K = 5.4127$. Bottom row. left panel: $\mathrm{Pe}_K = 10.8253$; middle panel: $\mathrm{Pe}_K = 21.6506$; right panel: $\mathrm{Pe}_K = 42.3012$.

method computes a solution that is much more accurate than that computed by the Upwind stabilized in the boundary layer region.

8.2.2 Active interface

In this section, we assume that the interface located at $z = 0.5$ is active and set $\kappa = 2$ and $\sigma = 1$. Moreover, the values of model coefficients are selected in such a way that the problem is diffusion-dominated in one subregion and advection-dominated in the other region. Specifically, in the first case of study we set $\mu = 1$, $\mathbf{v} = v_z\mathbf{e}_3$, $v_z = 1$, in Ω_1 and $\mu = 0.0325$, $\mathbf{v} = v_z\mathbf{e}_3$ in Ω_2, so that $\mathrm{Pe}_K|_{\Omega_1} = 0.0541$ and $\mathrm{Pe}_K|_{\Omega_2} = 1.6654$. In the second case of study we set $\mu = 1$, $v_z = 1$ in Ω_1 and $\mu = 0.008125$, $v_z = 1$ in Ω_2, so that $\mathrm{Pe}_K|_{\Omega_1} = 0.0541$ and $\mathrm{Pe}_K|_{\Omega_2} = 6.6618$. Thus, in both cases of study the problem is diffusion-dominated in Ω_1 and advection-dominated in Ω_2. Figure 8 shows a cross-sectional view of the reconstructed solution u_h^* along the z-axis. In both cases we see that: (a) the non stabilized and stabilized solutions correctly capture the sharp discontinuity at $z = 0.5$; (b) the non stabilized solution displays increasing instabilities in the boundary layer region at $z = 1$ as Pe_K increases; (c) the two stabilized solutions capture the boundary layer without any unphysical oscillations.

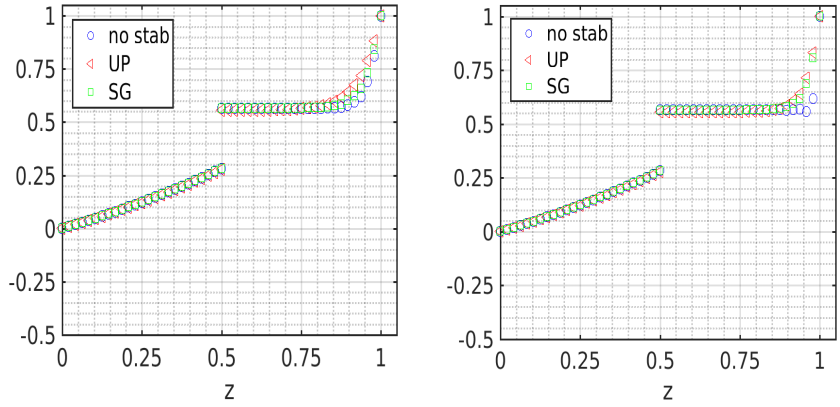

Figure 8 – 1D plot of the computed solution u_h^* along the z-axis. Blue circles: unstabilized solution. Green squares: SG stabilization. Red triangles: Upwind stabilization. u_h^* along the z-axis. Left panel: $\mu = 1$, $v_z = 1$ in Ω_1, $\mathrm{Pe}_K|_{\Omega_1} = 0.0541$; $\mu = 0.0325$, $v_z = 1$ in Ω_2, $\mathrm{Pe}_K|_{\Omega_2} = 1.6654$. Right panel: $\mu = 1$, $v_z = 1$ in Ω_1, $\mathrm{Pe}_K|_{\Omega_1} = 0.0541$; $\mu = 0.008125$, $v_z = 1$ in Ω_2, $\mathrm{Pe}_K|_{\Omega_2} = 6.6618$.

9 Conclusions and perspectives

In this work we have proposed, analyzed and numerically validated a novel dual mixed hybrid (DMH) finite element method (FEM), based on the Raviart-Thomas finite element space of lowest order (RT0), for the numerical approximation of a boundary value problem with diffusive, advective and reactive terms to be solved in a three-dimensional domain with transmission conditions across a selective interface.

The novel DMH-RT0 FEM belongs to the family of hybridizable discontinuous Galerkin (HDG) finite element methods for advection-diffusion-reaction problems (see [31], [16] and [12] for recent examples in the treatment of elliptic problems with interfaces and dominating convection). The new formulation combines in a unified framework a pair of Lagrange multipliers to account for the interface conditions, with the dual mixed hybrid method for the weak formulation and discretization of the problem. To stabilize the computation against advection dominance, an artificial diffusion is introduced along the streamline direction, as in the SUPG method.

The resulting scheme is a flexible and robust numerical approach for the treatment of heterogeneous problems where model coefficients may be subject to wide variations over the partitioned computational domain and sharp discontinuities of the primal variable and of the associated flux density may occur at the interface.

The unique solvability of the scheme is analyzed and optimal error estimates are proved with respect to the finite element discretization parameter using the abstract theory of saddle-point problems. An efficient implementation of the method within the computational platform MP-FEMOS is made

possible by the use of static condensation to eliminate the internal variables and the Lagrange multipliers for the dual variable at the interface in favor of the hybrid variable and of the Lagrange multiplier for the primal variable at the interface.

Extensive numerical tests demonstrate the theoretical conclusions and indicate that the proposed DMH-RT0 FEM is accurate and stable in the presence of marked interface jump discontinuities of both solution and associated normal flux. In the case of strongly dominating advective terms, the proposed method is capable to accurately resolve steep boundary and/or interior layers without introducing spurious unphysical oscillations or excessive smearing of the solution front.

Next objectives of the ongoing research activity on the proposed method include:

- performing simulations with a non-planar interface. This will allow us to better validate the performance of the method on a more complicated geometry than considered in Section 8, including corners and/or internal layers (see [47]);
- extending the implementation to domains with multiple interfaces. This will allow us to study more realistic physical situations such as the case of the interaction between two cellular compartments separated by an extracellular fluid [28] or the case of the design of advanced memories in nanoelectronics in which materials are characterized by the presence of localized defects [51];
- extending the mathematical model to nonlinear transmission conditions at the interface. This will allow us to study more realistic physical problems such as the case of semipermeable membranes [29] or biochemical reactions in cellular biology [54];
- extending the numerical approach and its application to transmission models to HDG methods (cf. [31]). This will allow us to benefit from the high flexibility of the HDG computational framework, in particular the possibility of adopting standard polynomial basis functions for *both* primal and dual variables, including the case of equal-order interpolation [17];
- extending the DMH numerical scheme to the case where the geometrical discretization of the domain Ω is *not* fitted with the interface Γ. This will allow us to combine the discontinuous features of the DMH method with the flexible and efficient computational framework of Extended Finite Elements (XFEM), as recently analyzed in [24] in the study of XFEM-based approximation of flow in fractured porous media;
- extending the theoretical analysis of the convergence of the scheme to include the artificial diffusion stabilization of Section 6. This will allow us to characterize the effect of the perturbation term $\boldsymbol{\mu}_K^*$ in (35) on the accuracy of the method as h is sufficiently small by estimating the introduced consistency error with the Strang Lemma [40, Chapter 5].

Acknowledgements

The authors gratefully acknowledge the anonymous Reviewer for useful comments and suggestions. Giovanna Guidoboni has been partially supported by the Chair Gutenberg funds of the Cercle Gutenberg (France), by the Labex IRMIA (University of Strasbourg, France) and by the award DMS 1853222/1853303 of the National Science Foundation (USA). Riccardo Sacco is a Member of the INdAM Research group GNCS and has been partially supported by Micron Semiconductor Italia S.r.l., statement of work #4505462139: "Modeling of tunneling and charging dynamics", contractors: Micron Semiconductor Italia S.r.l.; Dipartimento di Matematica Politecnico di Milano, Italy.

References

1. Computation of local Pèclet number for anisotropic mesh. https://fenicsproject.org/qa/9171/computation-of-local-peclet-number-for-anisotropic-mesh.
2. D. Addy, M. Pradas, M. Schmuck, and S. Kalliadasis. Diffuse-Interface Modelling of Flow in Porous Media. In *APS Meeting Abstracts*, November 2016.
3. P. Airoldi, A. G. Mauri, R. Sacco, and J. W. Jerome. Three-dimensional numerical simulation of ion nanochannels. *Journal of Coupled System and Multiscale Dynamics*, 3(1):57–65, 2015.
4. S. M. Amoroso, C. Monzio Compagnoni, A. Mauri, A. Maconi, A. S. Spinelli, and A. L. Lacaita. Semi-analytical model for the transient operation of gate-all-around charge-trap memories. *IEEE Transactions on Electron Devices*, 58(9):3116–3123, Sept 2011.
5. T. Arbogast and Z. Chen. On the implementation of mixed methods as nonconforming methods for second- order elliptic problems. *Mathematics of Computation*, 64(211):943–972, 1995.
6. D.N Arnold and F. Brezzi. Mixed and nonconforming finite element methods: implementation, postprocessing and error estimates. *Math. Modeling and Numer. Anal.*, 19(1):7–32, 1985.
7. R. E. Bank, J. F. Bürgler, W. Fichtner, and R. K. Smith. Some upwinding techniques for finite element approximations of convection-diffusion equations. *Numerische Mathematik*, 58(1):185–202, 1990.
8. F. Brezzi and M. Fortin. *Mixed and Hybrid Finite Element Methods*, volume 15 of *Springer Series in Computational Mathematics*. Springer-Verlag, New York, 1991.
9. F. Brezzi and L. D. Marini. A three-field domain decomposition method. In A. Quarteroni, J. Periaux, Y. A. Kuznetsov, and O .B. Widlund, editors, *Domain Decomposition Methods in Science and Engineering*, pages 27–34. American Mathematical Society, Providence, 1994.
10. F. Brezzi and L. D. Marini. Error estimates for the three-field formulation with bubble stabilization. *Math. Comp.*, 70(235):911–934, 2000.
11. A. N. Brooks and T. J.R. Hughes. Streamline upwind/Petrov-Galerkin formulations for convection dominated flows with particular emphasis on the incompressible Navier-Stokes equations. *Computer Methods in Applied Mechanics and Engineering*, 32(1):199 – 259, 1982.
12. Rommel Bustinza, Ariel L. Lombardi, and Manuel Solano. An anisotropic a priori error analysis for a convection-dominated diffusion problem using the hdg method. *Computer Methods in Applied Mechanics and Engineering*, 345:382 – 401, 2019.
13. A. Cangiani and R. Natalini. A spatial model of cellular molecular trafficking including active transport along microtubules. *Journal of Theoretical Biology*, 267(4):614 – 625, 2010.
14. P. Causin, M. Restelli, and R. Sacco. A simulation system based on mixed-hybrid finite elements for thermal oxidation in semiconductor technology. *Computer Methods in Applied Mechanics and Engineering*, 193(33–35):3687 – 3710, 2004.

15. H. Ceric, A. Hoessinger, T. Binder, and S. Selberherr. Modeling of segregation on material interfaces by means of the finite element method. In *Proceedings 4th Mathmod Vienna, February 2003, I. Troch, F. Breitenecker, eds.*, pages 139–145, 2003.
16. Huangxin Chen, Jingzhi Li, and Weifeng Qiu. Robust a posteriori error estimates for HDG method for convection2̌013diffusion equations . *IMA Journal of Numerical Analysis*, 36(1):437–462, 03 2015.
17. B. Cockburn. The Hybridizable Discontinuous Galerkin method. In *Proceedings of the International Congress of Mathematicians*, pages 2749–2775, 2010.
18. B. Cockburn, J. Gopalakrishnan, and R. Lazarov. Unified hybridization of discontinuous Galerkin, mixed, and continuous Galerkin methods for second order elliptic problems. *SIAM Journal on Numerical Analysis*, 47(2):1319–1365, 2009.
19. M. Crouzeix and P.-A. Raviart. Conforming and nonconforming finite element methods for solving the stationary Stokes equations I. *ESAIM: Mathematical Modelling and Numerical Analysis - Modélisation Mathématique et Analyse Numérique*, 7(R3):33 – 75, 1973.
20. B. M. Fraejis de Veubeke. Displacement and equilibrium models in the finite element method. In O. Zienkiewicz and G. Holister, editors, *Stress Analysis*, pages 145–197. John Wiley & Sons, New York, 1965.
21. J. Douglas and J. E. Roberts. Global estimates for mixed methods for second order elliptic equations. *Math. Comp.*, 44(169):39–52, 1985.
22. M. Farhloul and M. Fortin. A new mixed finite element for the Stokes and elasticity problems. *SIAM Journal on Numerical Analysis*, 30(4):971–990, 1993.
23. M. Farhloul and M. Fortin. Dual hybrid methods for the elasticity and the Stokes problems: a unified approach. *Numerische Mathematik*, 76(4):419–440, 1997.
24. B. Flemisch, A. Fumagalli, and A. Scotti. *A Review of the XFEM-Based Approximation of Flow in Fractured Porous Media*, pages 47–76. Springer International Publishing, Cham, 2016.
25. M. Fortin and A. S. Mounim. Mixed and hybrid finite element methods for convection-diffusion problems and their relationships with finite volume: The multi-dimensional case. *Journal of Mathematics Research*, 9(1):68–83, 2017.
26. T.-P. Fries and T. Belytschko. The extended/generalized finite element method: An overview of the method and its applications. *International Journal for Numerical Methods in Engineering*, 84(3):253–304, 2010.
27. D. Gilbarg and N. S. Trudinger. *Elliptic Partial Differential Equations of Second Order*. Classics in Mathematics. Springer-Verlag Berlin Heidelberg, 2001.
28. B. P. Graham and A. van Ooyen. Mathematical modelling and numerical simulation of the morphological development of neurons. *BMC Neuroscience*, 7((Suppl 1)):S1–S9, 2006.
29. J. Hron, M. Neuss-Radu, and P. Pustějovská. Mathematical modeling and simulation of flow in domains separated by leaky semipermeable membrane including osmotic effect. *Applications of Mathematics*, 56(1):51–68, Feb 2011.
30. T. J. R. Hughes, L. P. Franca, and M. Mallet. A new finite element formulation for computational fluid dynamics: Vi. convergence analysis of the generalized SUPG formulation for linear time-dependent multidimensional advective-diffusive systems. *Computer Methods in Applied Mechanics and Engineering*, 63(1):97 – 112, 1987.
31. L.N. T. Huynh, N.C. Nguyen, J. Peraire, and B.C. Khoo. A high-order hybridizable discontinuous galerkin method for elliptic interface problems. *International Journal for Numerical Methods in Engineering*, 93(2):183–200, 2013.
32. O. Kedem and A. Katchalsky. Thermodynamic analysis of the permeability of biological membranes to non-electrolytes. *Biochimica et Biophysica Acta*, 27:229 – 246, 1958.
33. S. Lee and V. Sundararaghavan. Multi-scale modeling of moving interface problems with flux and field jumps: Application to oxidative degradation of ceramic matrix composites. *International Journal for Numerical Methods in Engineering*, 85(6):784–804, 2011.
34. J.L. Lions and E. Magenes. *Non-homogeneous boundary value problems and applications*. Number v. 3 in Non-homogeneous Boundary Value Problems and Applications. Springer-Verlag, 1972.
35. V. Martin, J. Jaffré, and J. E. Roberts. Modeling fractures and barriers as interfaces for flow in porous media. *SIAM Journal on Scientific Computing*, 26(5):1667–1691, 2005.

36. A. G. Mauri, A. Bortolossi, G. Novielli, and R. Sacco. 3D finite element modeling and simulation of industrial semiconductor devices including impact ionization. *Journal of Mathematics in Industry*, 5:1–18, 2015. doi:10.1186/s13362-015-0015-z.
37. A. G. Mauri, R. Sacco, and M. Verri. Electro-thermo-chemical computational models for 3D heterogeneous semiconductor device simulation. *Applied Mathematical Modelling*, 39(14):4057–4074, 2014.
38. A. G. Mauri, L. Sala, P. Airoldi, G. Novielli, R. Sacco, S. Cassani, G. Guidoboni, B. A. Siesky, and A. Harris. Electro-fluid dynamics of aqueous humor production: simulations and new directions. *Journal for Modeling in Ophthalmology*, 2:48–58, 2016.
39. E. Onate and M. Manzan. Stabilization techniques for finite element analysis of convection-diffusion problems. Technical report, International Center for Numerical Methods in Engineering (CIMNE), Barcelona, Spain, 2000. Publication CIMNE No-183.
40. A. Quarteroni and A. Valli. *Numerical Approximation of Partial Differential Equations*. Lecture Notes in Mathematics. Springer-Verlag, 1994.
41. A. Quarteroni and A. Valli. *Domain decomposition methods for partial differential equations*. Numerical Mathematics Scientific Computation, Clarendon Press, 1999.
42. V. S. Rao and T. J. R. Hughes. On modelling thermal oxidation of silicon i: theory. *International Journal for Numerical Methods in Engineering*, 47(1-3):341–358, 2000.
43. V. S. Rao, T. J. R. Hughes, and K. Garikipati. On modelling thermal oxidation of silicon ii: numerical aspects. *International Journal for Numerical Methods in Engineering*, 47(1-3):359–377, 2000.
44. P. A. Raviart and J.M. Thomas. Dual finite element models for 2nd order elliptic problems. In R. Glowinski, E. Y. Rodin, and O. C. Zienkiewicz, editors, *Energy Methods in Finite Element Analysis*, pages 175–191. Wiley, New York, 1979.
45. P.A. Raviart and J.M. Thomas. A mixed finite element method for second order elliptic problems. In I. Galligani and E. Magenes, editors, *Mathematical Aspects of Finite Element Methods,I*. Springer-Verlag, Berlin, 1977.
46. J.E. Roberts and J.M. Thomas. Mixed and hybrid methods. In P.G. Ciarlet and J.L. Lions, editors, *Finite Element Methods, Part I*. North-Holland, Amsterdam, 1991. Vol.2.
47. H.-G. Roos, M. Stynes, and L. Tobiska. *Robust numerical methods for singularly perturbed differential equations*, volume 24. Springer, 2008.
48. W. L. C. Rutten. Selective electrical interfaces with the nervous system. *Annual Review of Biomedical Engineering*, 4:407–452, 2002.
49. R. Sacco, P. Airoldi, A. G. Mauri, and J. W. Jerome. Three-dimensional simulation of biological ion channels under mechanical, thermal and fluid forces. *Applied Mathematical Modelling*, 43:221 – 251, 2017.
50. J. M. Thomas. *Sur l'analyse numérique des mèthodes d'eléments finis hybrides et mixtes*. PhD thesis, Université Pierre et Marie Curie, 1977. Thése d'Etat.
51. P. Weckx, B. Kaczer, M. Toledano-Luque, T. Grasser, Ph. J. Roussel, H. Kukner, P. Raghavan, F. Catthoor, and G. Groeseneken. Defect-based methodology for workload-dependent circuit lifetime projections-application to SRAM. In *Reliability Physics Symposium (IRPS), 2013 IEEE International*, pages 3A–4. IEEE, 2013.
52. G. B. Wills and E. N. Lightfoot. Membrane selectivity. *AIChE Journal*, 7(2):273–276, 1961.
53. B. D. Wood, M. Quintard, and S. Whitaker. Calculation of effective diffusivities for biofilms and tissues. *Biotechnology and Bioengineering*, 77(5):495–516, 2002.
54. B. D. Wood and S. Whitaker. Cellular growth in biofilms. *Biotechnology and Bioengineering*, 64(6):656–670, 1999.
55. S. Yakovlev, D. Moxey, R. M. Kirby, and S. J. Sherwin. To cg or to hdg: A comparative study in 3d. *Journal of Scientific Computing*, 67(1):192–220, 2016.

A Efficient implementation of the DMH method

In this appendix, we illustrate how to implement the DMH-RT0 FEM (17) in a computationally efficient manner. To this end, we first discuss the properties of the linear algebraic

system and then describe in detail the static condensation procedure that allows us to eliminate the internal variables $u_i, \mathbf{J}_i$ and the Lagrange multipliers $\mathcal{J}_i$ in favor of $\widehat{u}_i$ and λ, $i = 1, 2$.

A.1 System reduction through static condensation

Functions belonging to the finite dimensional space $\mathcal{V}_h$ are completely discontinuous over $\mathcal{T}_h$. Similarly, functions belonging to the finite dimensional space $\mathcal{Q}_h$ are completely discontinuous over $\mathcal{F}_h$. These properties can be profitably exploited to implement the DMH-RT0 FEM in a very efficient manner through the use of static condensation. This procedure is basically a Gauss elimination algorithm that allows us to express all the variables of the numerical method as a function of a sole unknown, thereby reducing considerably the size of the linear algebraic system and enhancing the computational efficiency of the method. Static condensation, however, is not a feature specific of the DMH-RT0 FEM proposed in the present article, but is widely adopted in finite element formulations. We refer to [6, 8] for an introduction to static condensation in mixed and hybrid finite element methods, to [18,55] for an advanced use of static condensation in the context of Continuous and Hybridizable Discontinuous Galerkin methods and to [41] for a description of the use of static condensation as an algorithm to implement the method of Schur complement system. To apply static condensation to the DMH FEM it is convenient to write the linear algebraic system associated with problem (17) in full block form, which reads:

$$\begin{bmatrix} \mathtt{A}_1 & \mathtt{N}_1 & 0 & 0 & \mathtt{D}_1^T & 0 & 0 & 0 & 0 \\ \mathtt{P}_1 & \mathtt{R}_1 & 0 & 0 & 0 & 0 & 0 & 0 & 0 \\ 0 & 0 & \mathtt{A}_2 & \mathtt{N}_2 & 0 & \mathtt{D}_2^T & 0 & 0 & 0 \\ 0 & 0 & \mathtt{P}_2 & \mathtt{R}_2 & 0 & 0 & 0 & 0 & 0 \\ \mathtt{D}_1 & 0 & 0 & 0 & -\mathtt{M}_{\Sigma_1} & 0 & -\mathtt{E}_1^T & 0 & 0 \\ 0 & 0 & \mathtt{D}_2 & 0 & 0 & -\mathtt{M}_{\Sigma_2} & 0 & -\mathtt{E}_2^T & 0 \\ 0 & 0 & 0 & 0 & \mathtt{E}_1 & 0 & 0 & 0 & -\mathtt{U}_1^T \\ 0 & 0 & 0 & 0 & 0 & \mathtt{E}_2 & 0 & 0 & -\kappa\mathtt{U}_2^T \\ 0 & 0 & 0 & 0 & 0 & 0 & \mathtt{U}_1 & \mathtt{U}_2 & 0 \end{bmatrix} \begin{bmatrix} \mathbf{J}_1 \\ \mathbf{u}_1 \\ \mathbf{J}_2 \\ \mathbf{u}_2 \\ \widehat{\mathbf{u}}_1 \\ \widehat{\mathbf{u}}_2 \\ \mathbf{j}_1 \\ \mathbf{j}_2 \\ \boldsymbol{\lambda} \end{bmatrix} = \begin{bmatrix} \mathbf{0} \\ \mathbf{b}_1 \\ \mathbf{0} \\ \mathbf{b}_2 \\ \mathbf{b}_{\Sigma_1} \\ \mathbf{b}_{\Sigma_2} \\ \mathbf{0} \\ \mathbf{0} \\ \mathbf{b}_\sigma \end{bmatrix}. \tag{40}$$

In the equation system (40), $\mathbf{J}_i$, $\mathbf{u}_i$, $i = 1, 2$, denote the vectors of the degrees of freedom for the internal variables $\mathbf{J}_h$ and u_h inside the partitioned triangulations $\mathcal{T}_{h,i}$, $i = 1, 2$. In particular, denoting by $\mathtt{NE}_1$ the number of tetrahedra in $\mathcal{T}_{h,1}$ and by $\mathtt{NE}_2$ the number of tetrahedra in $\mathcal{T}_{h,2}$, we notice that $\mathbf{J}_1$ is subdivided into a collection of $\mathtt{NE}_1$ vectors of size equal to 4 and $\mathbf{u}_1$ has size equal to $\mathtt{NE}_1$; analogously, $\mathbf{J}_2$ is subdivided into a collection of $\mathtt{NE}_2$ vectors of size equal to 4 and $\mathbf{u}_2$ has size equal to $\mathtt{NE}_2$. In the same spirit, matrix $\mathtt{A}_1$ has a block diagonal structure of size $\mathtt{NE}_1$, where each block is the 4×4 flux matrix corresponding to an element of $\mathcal{T}_{h,1}$, whereas matrix $\mathtt{A}_2$ has a block diagonal structure of size $\mathtt{NE}_2$, where each block is the 4×4 flux matrix corresponding to an element of $\mathcal{T}_{h,2}$. Similar considerations apply to the rectangular block matrices $\mathtt{P}_i$ and $\mathtt{N}_i := \mathtt{H}_i - \mathtt{P}_i^T$, $i = 1, 2$, and to the block matrices $\mathtt{R}_i$, $i = 1, 2$, that have a diagonal structure, each entry corresponding to an element of $\mathcal{T}_{h,1}$ and $\mathcal{T}_{h,2}$, respectively. The unknown vectors $\widehat{\mathbf{u}}_i$, instead, contain the degrees of freedom of the hybrid variables $\widehat{u}_{h,i}$, $i = 1, 2$, associated with each face of $\mathcal{F}_{h,i}$, $i = 1, 2$, and for this reason the size of $\widehat{\mathbf{u}}_1$ is equal to $\mathtt{NF}_1$ and the size of $\widehat{\mathbf{u}}_2$ is equal to $\mathtt{NF}_2$, where $\mathtt{NF}_1$ and $\mathtt{NF}_2$ denote the number of faces in $\mathcal{F}_{h,1}$ and $\mathcal{F}_{h,2}$, the faces belonging to the interface Γ being counted twice. The unknown vectors $\mathbf{j}_i$, $i = 1, 2$, contain the degrees of freedom of the flux Lagrange multipliers $\mathcal{J}_{h,i}$, $i = 1, 2$, associated with each face of $\mathcal{F}_{h,\Gamma,1}$ and $\mathcal{F}_{h,\Gamma,2}$, respectively, and therefore their sizes are both equal to $\mathtt{NF}_\Gamma$, where $\mathtt{NF}_\Gamma$ denotes the number of faces in $\mathcal{F}_{h,\Gamma}$. Finally, the unknown vector $\boldsymbol{\lambda}$ contains the degrees of freedom of the segregation condition Lagrange multiplier λ_h associated with each face of $\mathcal{F}_{h,\Gamma}$, and therefore has size equal to $\mathtt{NF}_\Gamma$. The matrices $\mathtt{D}_i$, $i = 1, 2$, enforce the continuity of $\mathbf{J}_{h,i}\cdot\mathbf{n}_i$ across interelement boundaries in each triangulation $\mathcal{T}_{h,i}$. The matrices $\mathtt{M}_{\Sigma_i}$, $i = 1, 2$, enforce the continuity of the Robin boundary boundary conditions (1e) on each face of Σ_i. The matrices $\mathtt{E}_i$, $i = 1, 2$, enforce the identity between $\mathbf{J}_{h,i} \cdot \mathbf{n}_i$ and the

Lagrange multiplier $\mathcal{J}_{h,i}$ across each face belonging to $\mathcal{F}_{h,\Gamma,i}$, $i = 1, 2$. The matrices $\mathtt{U}_1$ and $\mathtt{U}_2$ enforce the transmission condition (1c) across each face of $\mathcal{F}_{h,\Gamma}$ whereas the matrices $-\mathtt{U}_1^T$ and $-\kappa\mathtt{U}_2^T$ enforce the segregation condition (1d) across each face of $\mathcal{F}_{h,\Gamma}$. In analogy to what happens for the matrices associated with the internal degrees of freedom in each partitioned triangulation, also the matrices $\mathtt{D}_i$, $\mathtt{M}_{\Sigma_i}$, $\mathtt{E}_i$ and $\mathtt{U}_i$ have a block structure, each block corresponding to a face of $\mathcal{F}_{h,i}$, $i = 1, 2$. To conclude, the right-hand side vectors $\mathbf{b}_i$, $\mathbf{b}_{\Sigma_i}$ and $\mathbf{b}_\sigma$, contain the contributions due to the source term g in (1a), of the boundary terms β_i in (1e) and of the interface flux term $-\sigma$ in (1c), respectively.

A.1.1 Elimination of the internal variables $\mathbf{J}_h$ *and* u_h

The first and second equations in the block linear system (40) read:

$$\mathtt{A}_1\mathbf{J}_1 + \mathtt{N}_1\mathbf{u}_1 + \mathtt{D}_1^T\widehat{\mathbf{u}}_1 = \mathbf{0} \tag{41a}$$

$$\mathtt{P}_1\mathbf{J}_1 + \mathtt{R}_1\mathbf{u}_1 = \mathbf{g}_1, \tag{41b}$$

whereas the third and fourth equations in the block linear system (40) read:

$$\mathtt{A}_2\mathbf{J}_2 + \mathtt{N}_2\mathbf{u}_2 + \mathtt{D}_2^T\widehat{\mathbf{u}}_2 = \mathbf{0} \tag{42a}$$

$$\mathtt{P}_2\mathbf{J}_2 + \mathtt{R}_2\mathbf{u}_2 = \mathbf{g}_2. \tag{42b}$$

The two systems (41) and (42) have a *local* nature, that is, the unknown vector pairs $(\mathbf{J}_i, \mathbf{u}_i)$, $i = 1, 2$, are associated with each tetrahedron K belonging to $\mathcal{T}_{h,1}$ and $\mathcal{T}_{h,2}$, respectively. In particular, we see that the 4×4 flux matrices $\mathtt{A}_i$, $i = 1, 2$, are symmetric and positive definite, so that (41a) and (42a) can be solved to obtain:

$$\mathbf{J}_1 = -\mathtt{A}_1^{-1}\left[\mathtt{N}_1\mathbf{u}_1 + \mathtt{D}_1^T\widehat{\mathbf{u}}_1\right], \tag{43a}$$

$$\mathbf{J}_2 = -\mathtt{A}_2^{-1}\left[\mathtt{N}_2\mathbf{u}_2 + \mathtt{D}_2^T\widehat{\mathbf{u}}_2\right]. \tag{43b}$$

Then, we can substitute the above expressions in (41b) and (42b) to get:

$$-\mathtt{P}_1\mathtt{A}_1^{-1}\left[\mathtt{N}_1\mathbf{u}_1 + \mathtt{D}_1^T\widehat{\mathbf{u}}_1\right] + \mathtt{R}_1\mathbf{u}_1 = \mathbf{g}_1, \tag{44a}$$

$$-\mathtt{P}_2\mathtt{A}_2^{-1}\left[\mathtt{N}_2\mathbf{u}_2 + \mathtt{D}_2^T\widehat{\mathbf{u}}_2\right] + \mathtt{R}_2\mathbf{u}_2 = \mathbf{g}_2. \tag{44b}$$

Letting

$$\mathtt{M}_i := \mathtt{R}_i - \mathtt{P}_i\mathtt{A}_i^{-1}\mathtt{N}_i = \mathtt{R}_i + \mathtt{P}_i\mathtt{A}_i^{-1}\mathtt{P}_i^T - \mathtt{P}_i\mathtt{A}_i^{-1}\mathtt{H}_i, \qquad i = 1, 2,$$

equations (44) become:

$$\mathtt{M}_1\mathbf{u}_1 - \mathtt{P}_1\mathtt{A}_1^{-1}\mathtt{D}_1^T\widehat{\mathbf{u}}_1 = \mathbf{g}_1, \tag{45a}$$

$$\mathtt{M}_2\mathbf{u}_2 - \mathtt{P}_2\mathtt{A}_2^{-1}\mathtt{D}_2^T\widehat{\mathbf{u}}_2 = \mathbf{g}_2. \tag{45b}$$

Matrices $\mathtt{M}_i$ have size 1×1 and are invertible because of assumption (9c). Thus, equations (45) can be solved to obtain:

$$\mathbf{u}_1 = \mathtt{M}_1^{-1}\left[\mathtt{P}_1\mathtt{A}_1^{-1}\mathtt{D}_1^T\widehat{\mathbf{u}}_1 + \mathbf{g}_1\right], \tag{46a}$$

$$\mathbf{u}_2 = \mathtt{M}_2^{-1}\left[\mathtt{P}_2\mathtt{A}_2^{-1}\mathtt{D}_2^T\widehat{\mathbf{u}}_2 + \mathbf{g}_2\right]. \tag{46b}$$

We can plug expressions (46) back into (43) to obtain the following affine equations for the degrees of freedom of the dual variable associated with each element $K \in \mathcal{T}_{h,i}$, $i = 1, 2$:

$$\mathbf{J}_1 = \mathtt{L}_1\widehat{\mathbf{u}}_1 + \mathbf{b}_1, \tag{47a}$$

$$\mathbf{J}_2 = \mathtt{L}_2\widehat{\mathbf{u}}_2 + \mathbf{b}_2, \tag{47b}$$

where:

$$\mathtt{L}_1 := -\mathtt{A}_1^{-1}\left[\mathtt{N}_1\mathtt{M}_1^{-1}\mathtt{P}_1\mathtt{A}_1^{-1}\mathtt{D}_1^T + \mathtt{D}_1^T\right], \tag{47c}$$

$$\mathbf{b}_1 := -\mathtt{A}_1^{-1}\mathtt{N}_1\mathtt{M}_1^{-1}\mathbf{g}_1, \tag{47d}$$

$$\mathtt{L}_2 := -\mathtt{A}_2^{-1}\left[\mathtt{N}_2\mathtt{M}_2^{-1}\mathtt{P}_2\mathtt{A}_2^{-1}\mathtt{D}_2^T + \mathtt{D}_2^T\right], \tag{47e}$$

$$\mathbf{b}_2 := -\mathtt{A}_2^{-1}\mathtt{N}_2\mathtt{M}_2^{-1}\mathbf{g}_2. \tag{47f}$$

A.1.2 Elimination of the interface Lagrange multipliers $\mathcal{J}_{i,h}$, $i = 1, 2$

Restricting the fifth equation in the block linear system (40) to the faces belonging to $\mathcal{F}_{h,\Gamma,1}$ yields

$$\mathtt{D}_1\mathbf{J}_1 - \mathtt{E}_1^T\mathbf{j}_1 = \mathbf{0}, \tag{48a}$$

whereas the restriction of the sixth equation in the block linear system (40) to the faces that belong to $\mathcal{F}_{h,\Gamma,2}$ yields

$$\mathtt{D}_2\mathbf{J}_2 - \mathtt{E}_2^T\mathbf{j}_2 = \mathbf{0}. \tag{48b}$$

Since test functions μ_h and approximate multipliers $\mathcal{J}_h$ belong to the same discrete space $M(F)$ defined in (14c), equations (48a) and (48b) are uniquely solvable for each face F belonging to the interface Γ, and give:

$$\mathbf{j}_1 = (\mathtt{E}_1^T)^{-1}\mathtt{D}_1\mathbf{J}_1, \tag{48c}$$

$$\mathbf{j}_2 = (\mathtt{E}_2^T)^{-1}\mathtt{D}_2\mathbf{J}_2, \tag{48d}$$

where $\mathbf{J}_1$ and $\mathbf{J}_2$ are given by (47). Also, since functions in the RT0 space (14a) satisfy the property

$$\mathbf{V}(K)\cdot\mathbf{n}_{\partial K}|_{F\in\partial K} = M(F) \qquad \forall K \in \mathcal{T}_h \qquad F \in \partial K,$$

equations (48c) and (48d) assume the particularly simple form:

$$\mathcal{J}_{1,h}|_F = \mathbf{J}_{1,h}\cdot\mathbf{n}_1|_F \qquad \forall F \in \mathcal{F}_{h,\Gamma,1}, \tag{48e}$$

$$\mathcal{J}_{2,h}|_F = \mathbf{J}_{2,h}\cdot\mathbf{n}_2|_F \qquad \forall F \in \mathcal{F}_{h,\Gamma,2}. \tag{48f}$$

A.1.3 Elimination of the hybrid variables on the interface Γ

The seventh equation in the block linear system (40) yields

$$\mathtt{E}_1\widehat{\mathbf{u}}_1 - \mathtt{U}_1^T\boldsymbol{\lambda} = \mathbf{0}, \tag{49a}$$

whereas the eigth equation in the block linear system (40) yields

$$\mathtt{E}_2\widehat{\mathbf{u}}_2 - \kappa\mathtt{U}_2^T\boldsymbol{\lambda} = \mathbf{0}. \tag{49b}$$

Using the same argument as for the variable $\mathcal{J}_h$, we see that equations (49) are uniquely solvable for each face F belonging to the interface Γ, and give:

$$\widehat{\mathbf{u}}_1 = \mathtt{E}_1^{-1}\mathtt{U}_1^T\boldsymbol{\lambda}, \tag{50a}$$

$$\widehat{\mathbf{u}}_2 = \kappa\mathtt{E}_2^{-1}\mathtt{U}_2^T\boldsymbol{\lambda}. \tag{50b}$$

We notice that equations (50) allow to express the segregation condition (1d) in the DMH formulation in the same manner as in the 3F method.

A.1.4 Construction of the linear algebraic system

Having expressed the internal variable $\mathbf{J}_h$ in favor of the hybrid variable $\widehat{u}_h$, the Lagrange multiplier $\mathcal{J}_h$ in favor of $\mathbf{J}_h$ on Γ and the hybrid variable $\widehat{u}_h$ in favor of the Lagrange multiplier λ_h on Γ, we proceed as follows:

(step a) we use the fifth equation in the block linear system (40) to enforce the interelement continuity of $\mathbf{J}_{1,h} \cdot \mathbf{n}_1|_F$ at each $F \in \mathcal{F}_{h,int,1}$ and the boundary condition (1e) at each $F \in \mathcal{F}_{h,\Sigma,1}$.

(step b) we use the sixth equation in the block linear system (40) to enforce the interelement continuity of $\mathbf{J}_{2,h} \cdot \mathbf{n}_2|_F$ at each $F \in \mathcal{F}_{h,int,2}$ and the boundary condition (1e) at each $F \in \mathcal{F}_{h,\Sigma,2}$;

(step c) we use the ninth equation in the block linear system (40) to enforce the transmission condition (1c) at each $F \in \mathcal{F}_{h,\Gamma}$.

A graphical representation of each of the above three steps is shown in Figure 9.

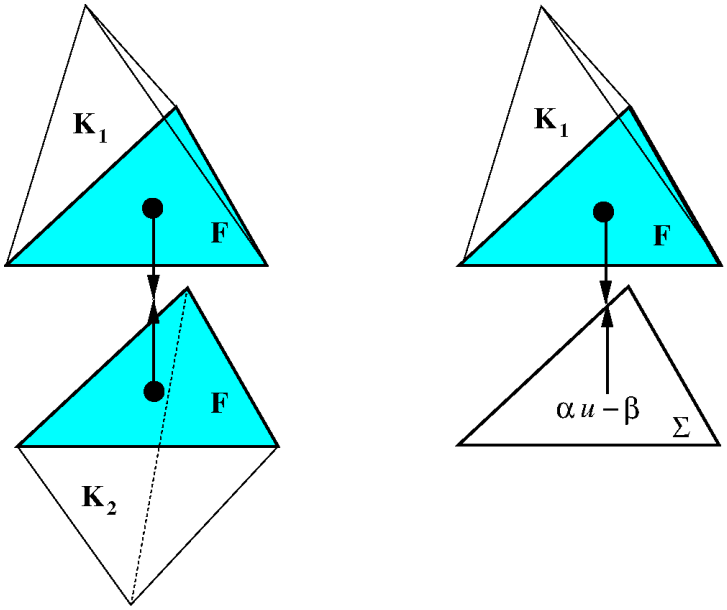

Figure 9 – Interelement continuity of $\mathbf{J}_h \cdot \mathbf{n}|_F$. Left panel: $F = \partial K_1 \cap \partial K_2$ (internal face). Right panel: $F = \partial K_1 \cap \Sigma$ (boundary face). The arrows represent the degree of freedom of $\mathbf{J}_h|_{K_i}$ associated with face F of element K_i, $i = 1, 2$ (left panel) and $i = 1$ (right panel). In the case where F is a boundary face the role of $\mathbf{J}_h|_{K_2} \cdot \mathbf{n}$ is played by the Robin boundary condition $\alpha u - \beta$.

The application of the sequence of steps (a), (b) and (c) leads to the construction of the following linear reduced system for the DMH-RT0 FEM

$$\mathtt{K}\mathbf{U} = \mathbf{t}, \tag{51}$$

where $\mathbf{U} \in \mathbb{R}^{\mathtt{NF}}$ is the vector of degrees of freedom represented by the values of $\widehat{u}_h$ on each face of $\mathcal{F}_h$, excluding those belonging to Γ, and the values of λ_h on each face belonging to Γ, $\mathtt{K} \in \mathbb{R}^{\mathtt{NF}\times\mathtt{NF}}$ is the stiffness matrix and $\mathbf{t} \in \mathbb{R}^{\mathtt{NF}}$ is the load vector, with $\mathtt{NF}$ denoting the

number of faces of $\mathcal{F}_h$. Each equation in (51) can be written in explicit form as

$$\mathtt{K}_{F,F}\mathbf{U}_F + \sum_{G\in\mathtt{Adj}(F)} \mathtt{K}_{F,G}\mathbf{U}_G = \mathbf{t}_F \qquad F = 1,\ldots,\mathtt{NF}, \tag{52}$$

where $\mathtt{Adj}(F)$ denotes the set of faces $G \in \mathcal{F}_h$ that have a vertex in common with the closure of F. We notice that each row of system (51) corresponding to an internal face F has 7 nonzero entries (cf. Figure 9, left panel) whereas each row of system (51) corresponding to a boundary face F has 4 nonzero entries (cf. Figure 9, right panel).

Remark 6 The unique solvability of (51) is a consequence of Theorem 2.

Remark 7 The assembly of the stiffness matrix K and of the load vector $\mathbf{t}$ in (51) can be conducted as in a standard displacement-based computer code using piecewise linear finite elements for the approximation of the primal variable u. In particular, a `for` loop is performed over the elements $K \in \mathcal{T}_h$ and for each element the *local* 4×4 stiffness matrix $\mathtt{L}_i^K$ and the *local* 4×1 load vector $\mathbf{t}_i^K = -\mathbf{b}_i^K$, $i = 1, 2$, are computed using (47). Then, the assembly phase consists of the following `Matlab` coding:

```
for Iloc=1:4,
    I = Lel(K,Iloc);
    for Jloc=1:4
        J = Lel(K,Jloc);
        if (Iloc==Jloc)
           GlobStiffMat(I,I) = GlobStiffMat(I,I) + ...
           LocStiffMat(Iloc,Iloc);
        else
           GlobStiffMat(I,J) = LocStiffMat(Iloc,Jloc);
        end
    end
    GlobLoadVec(I) = GlobLoadVec(I) + LocLoadVec(Iloc);
end
```

In the above code, K indicates the global index of element K in the mesh structure, Lel is the connectivity matrix such that Lel(K,i), i=1,2,3,4 contains the global index of the face of K locally numbered by i. In addition, GlobStiffMat and GlobLoadVec are the global stiffness matrix and global load vector, respectively, whereas LocStiffMat and LocLoadVec are their local counterparts. We notice that the assembly in the DMH-RT0 FEM is performed on a face-oriented basis, whereas in the standard FEM the assembly is performed on a vertex-oriented basis.

A.1.5 Post-processing

Once the reduced system (51) is solved, the values of $\widehat{u}_h$ on each face of $\mathcal{F}_{h,\Gamma,i}$, $i = 1, 2$, can be computed by means of (50). Then, the internal variables $\mathbf{J}_h$ and u_h are recovered using (47) and (46) over each $K \in \mathcal{T}_h$.